Tectonics®

RESEARCH ARTICLE
10.1029/2021TC007057

Key Points:

- First arrival of Asian detritus into the Central Myanmar Basin occurred after the earliest late Eocene and by the early Oligocene, thus constraining the time of WBT-Asia collision
- Our low temperature thermochronological study of the Indo-Burman Ranges indicates exhumation in the early-mid Eocene and around the Oligo-Miocene boundary

Supporting Information:

Supporting Information may be found in the online version of this article.

Correspondence to:

X. Luan,
xluan@sdust.edu.cn

Citation:

Najman, Y., Sobel, E. R., Millar, I., Luan, X., Zapata, S., Garzanti, E., et al. (2022). The timing of collision between Asia and the West Burma Terrane, and the development of the Indo-Burman Ranges. *Tectonics*, *41*, e2021TC007057. https://doi.org/10.1029/2021TC007057

Received 2 SEP 2021
Accepted 5 JUN 2022

The Timing of Collision Between Asia and the West Burma Terrane, and the Development of the Indo-Burman Ranges

Yani Najman[1], Edward R. Sobel[2], Ian Millar[3], Xiwu Luan[4], Sebastian Zapata[5], Eduardo Garzanti[6], Mauricio Parra[7], Giovanni Vezzoli[6], Peng Zhang[8], Day Wa Aung[9], Saw Mu Tha Lay Paw[10], and Thae Naung Lwin[9]

[1]Lancaster Environment Centre, Lancaster University, Lancaster, UK, [2]Institute of Geosciences, Universitat Potsdam, Potsdam-Golm, Germany, [3]NERC Isotope Geosciences Lab, BGS Keyworth, Keyworth, UK, [4]College of Earth Science and Engineering, Shandong University of Science and Technology, Qingdao, China, [5]Smithsonian Tropical Research Institute, Center for Tropical Paleocology and Archaeology, Panama, Panama, [6]Department of Earth and Environmental Sciences, Università di Milano-Bicocca, Milano, Italy, [7]Universidada de Sao Paulo, Institute for Energy and Environment, Sao Paulo, Brazil, [8]China University of Geosciences, Wuhan, China, [9]Geology Department, University of Yangon, Yangon, Myanmar, [10]Independent, Yangon, Myanmar

Abstract The West Burma Terrane (WBT) is a small terrane bounded to the east by the Asian Sibumasu Block and to the west by the Indo-Burman Ranges (IBR), the latter being an exhumed accretionary prism that formed during subduction of Indian oceanic lithosphere beneath Asia. Understanding the geological history of the WBT is important for reconstruction of the closure history of the Tethys Ocean and India-Asia collision. Currently there are major discrepancies in the proposed timings of collision between the WBT with both India and Asia; whether the WBT collided with India or Asia first is debated, and proposed timings of collisions stretch from the Mesozoic to the Cenozoic. We undertook a multi-technique provenance study involving petrography, detrital zircon U-Pb and Hf analyses, rutile U-Pb analyses and Sr-Nd bulk rock analyses on sediments of the Central Myanmar Basins of the WBT. We determined that the first arrival of Asian material into the basin occurred after the earliest late Eocene and by the early Oligocene, thus placing a minimum constraint on the timing of WBT-Asia collision. Our low temperature thermochronological study of the IBR records two periods of exhumation, in the early-middle Eocene, and at the Oligo-Miocene boundary. The Eocene event may be associated with the collision of the WBT with India. The later event at the Oligo-Miocene boundary may be associated with changes in wedge dynamics resulting from increased sediment supply to the system; however a number of other possible causes provide equally plausible explanations for both events.

Plain Language Summary Closure of the ancient Tethys Ocean by collision of various continental fragments culminated in the formation of the Himalayan mountain belt. A knowledge of the timing of collision of the various terranes is important to reconstruct the geological history of the region. The timing of the collision of the West Burma Terrane with both India and Asia is debated. We show that material eroded from Asia is first recorded in the Central Myanmar Basin of the West Burma Terrane after the earliest late Eocene and by the early Oligocene, providing a minimum time of docking of these continental fragments. We show two periods of exhumation of the exhumed accretionary prism of the Indo-Burman Ranges, in the early-middle Eocene and at the Oligo-Miocene boundary. These events may be associated with the collision of the West Burma Terrane and India, and changes in wedge dynamics, respectively, but other causes are equally plausible.

1. Introduction

The West Burma Terrane (WBT, Figure 1) is a small terrane, roughly coincident with the geographic borders of Myanmar. It consists of the Cretaceous-Cenozoic Wuntho-Popa Arc (WPA) and associated Central Myanmar forearc and backarc basins (CMB), separated from the Asian Sibumasu terrane to the east by the Sagaing Fault, and flanked to the west by the exhumed accretionary prism of the Indo-Burman Ranges (IBR).

Knowledge of the evolution of the WBT is important for understanding the geological history of the closure of the Tethys Ocean and stages of the India-Asia collision. Yet our current understanding is rudimentary. From Paleozoic times onward, various continental fragments including the WBT rifted from Gondwana and drifted north across the Tethys, accreting to the southern margin of Asia. Within this context, a number of researchers consider that the WBT was part of Asia by early Mesozoic or early Cenozoic times (see discussion in Barber

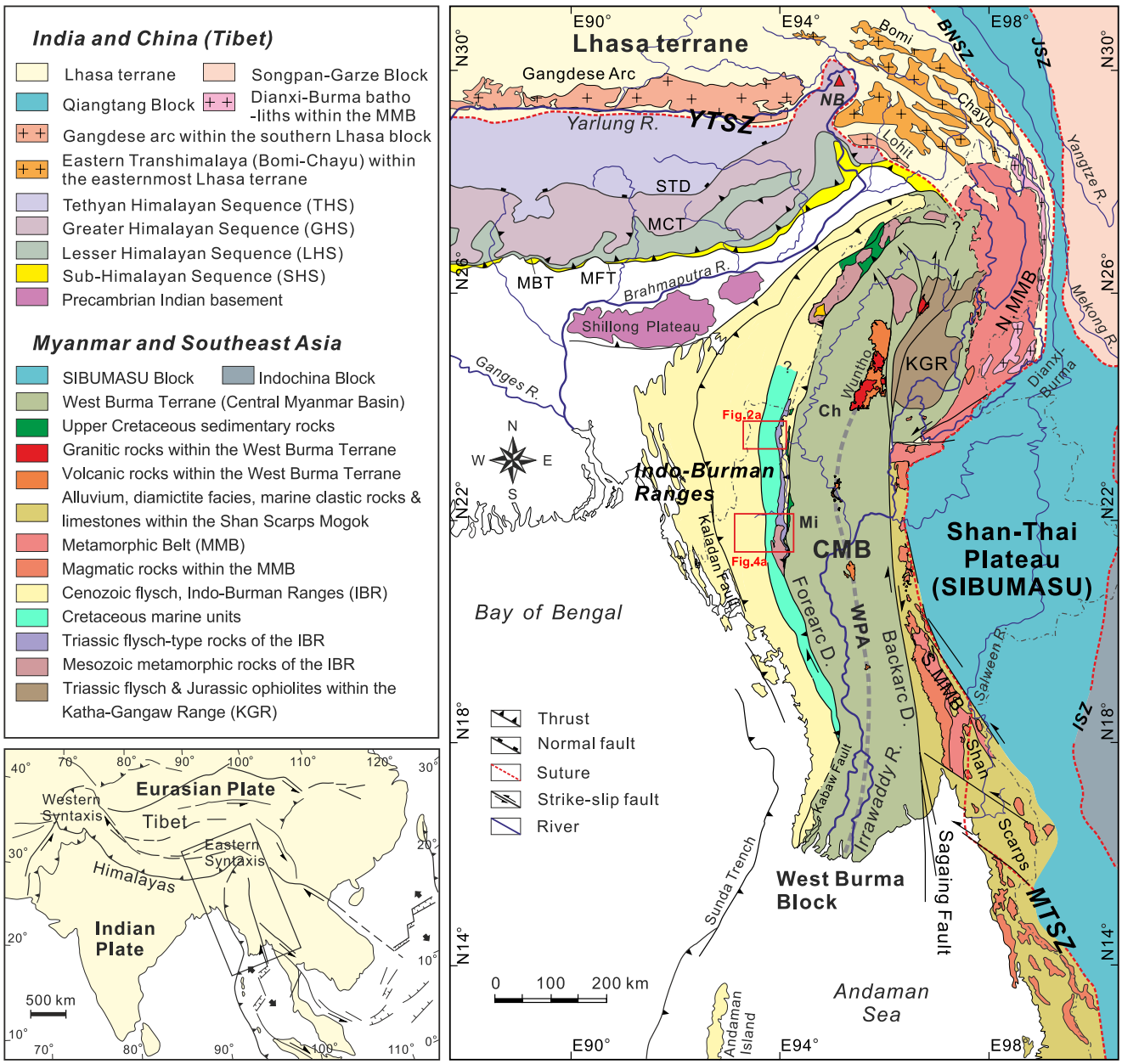

Figure 1. Geological map of Myanmar, also showing study areas of the age elevation profiles (Figures 2 and 4). Map is adapted from Mitchell et al. (2012) and Robinson et al. (2014), and references therein.

et al., 2017; Hall, 2012), which subsequently collided with India. Conversely, new paleomagnetic data suggest that the WBT lay at 5°S in the Late Cretaceous and 4°N in the late Eocene; the WBT collided with India in the early Cenozoic, followed by later collision with Asia (Westerweel et al., 2019, and see also Morley et al., 2020). However, as pointed out by Morley et al. (2021), this Late Eocene location requires rapid northward motion of the WBT in order for the terrane to reach its present position; such a trajectory should have left clear evidence of tectonic activity between the eastern margin of the WBT and the Asian margin of Sibumasu, which is not clearly observed.

In this paper, we investigate two aspects of the geology of the WBT that can be used to constrain the geological history of the terrane. First we research the provenance of the CMB, using it to determine when Asian material first arrived on the WBT and thus place constraints on when the two blocks collided. Previous work has proposed first arrival of Asian material into the CMB in late Eocene times (Licht et al., 2018), Oligocene times (Arboit

et al., 2021; Zhang et al., 2021) or not until the Miocene (Westerweel et al., 2020). Second, we determine the timing of uplift of the IBR, exhumation of which has been debatably linked to collision of the WBT with India (e.g., Aitchison et al., 2007; Morley, 2009; Morley et al., 2020; Verard et al., 2017). Previous work has indicated there is tentative evidence of IBR exhumation in the Eocene, with more substantial exhumation around the Oligo-Miocene boundary (Licht et al., 2018; Najman et al., 2020).

In this study, we undertook a second IBR age elevation transect >200 km north of our previous transect (Najman et al., 2020), and undertook thermal modeling of data from our previous transect. We aimed to assess the regional cooling history and to determine if rapid exhumation of the IBR in the Eocene, as we previously tentatively proposed, could be confirmed. Second, we undertook more provenance analyses in the CMB to narrow the data gap over which the timing of first arrival of Asian material that we previously identified (Zhang et al., 2021) occurred.

2. Geological Background

2.1. Geology of Myanmar

The geomorphology of Myanmar, closely tied to the geology, consists of four main divisions (Figure 1): the highlands to the north, the Shan Thai Plateau to the east, the IBR to the west, and the CMB in the center.

2.1.1. Sibumasu

Both the northern Highlands and the Shan Thai Plateau are part of the Asian Sibumasu Block.

Low to high grade metamorphic rocks of the Mogok Metamorphic Belt (MMB) and spatially associated granites are located in the northern Highlands of Myanmar, with a thin sliver of MMB rocks trending north-south along the length of the eastern margin of the CMB, separated from it by the Sagaing Fault. Metamorphism occurred from latest Cretaceous to Early Miocene, interpreted to be associated with India-Sibumasu collision (Barley et al., 2003; Lamont et al., 2021; Searle et al., 2020). Subsequent cooling and exhumation took place in the Late Oligo-Miocene (Bertrand et al., 2001). The granitoids, such as the Dianxi-Burma Batholiths of the MMB and the Bomi-Chayu Batholiths of the Eastern Transhimalaya, are of Cretaceous-Paleogene age (e.g., Liang et al., 2008). Sibumasu's Shan-Thai plateau is separated from the CMB by the Sagaing Fault. It is characterized by Cambrian-Mesozoic clastic sedimentary rocks, limestones and subordinate volcanics (e.g., Mitchell et al., 2012). On the western flank of the Shan Thai Plateau, a thin sliver of MMB extends from the north.

2.1.2. The Indo-Burman Ranges

The IBR is a north-south trending, west-vergent, thin-skinned fold-thrust belt (e.g., Betka et al., 2018) located on the western margin of the WBT, adjacent to the CMB (Figure 1). It is an exhumed accretionary prism affected by the hyper-oblique subduction of Tethyan lithosphere and final collision of India beneath and with the WBT (Morley et al., 2020; Luan et al., 2021). The eastern Inner side of the IBR consists of Cretaceous-middle Eocene deep marine rocks (including the Falam Fm., Morley et al., 2020) and some Late Eocene-Oligocene conglomerates (e.g., Aitchison et al., 2019; Ghose et al., 2014), while the western Outer belt extends to Neogene shallow marine and younger fluvial facies (e.g., Naing et al., 2014). The core of the IBR exposes Burmese "basement" of Kanpetlet schists, and its probable unmetamorphosed equivalent of the Triassic Pane Chaung turbidites (Morley et al., 2020), as well as early Cretaceous ophiolitic fragments (e.g., Socquet et al., 2002). Major Cenozoic structures within the Burmese portion of the range include the Kabaw, Kheng, and Kaladan faults. In our study area, deformation is driven by folds and west-vergent thrusts that have a component of dextral transpression (e.g., Mitchell et al., 2010; Morley et al., 2020). Our profile crosses four faults, discussed in Section 4.1.1.

2.1.3. The Central Myanmar Basins (CMB)

The CMB is a forearc-backarc basin couplet divided by the mid Cretaceous-Eocene Wuntho Popa arc (WPA) (e.g., Licht et al., 2020; P. Zhang et al., 2017). The forearc is divided into the Chindwin Sub-basin to the north and the Minbu Sub-basin to the south. The backarc is subdivided into the Shwebo, northern Minwun and Myitkina-Katha Sub-basins to the north and the Pegu Basin to the south. According to Licht et al. (2018), the forearc basins were partitioned, with different geological histories, from late Eocene times. Today, the Ayeyawady (Irrawaddy) River flows down the CMB from its headwaters in the MMB to the north of the basin.

Table 1
Summary of Central Myanmar Basins Stratigraphy

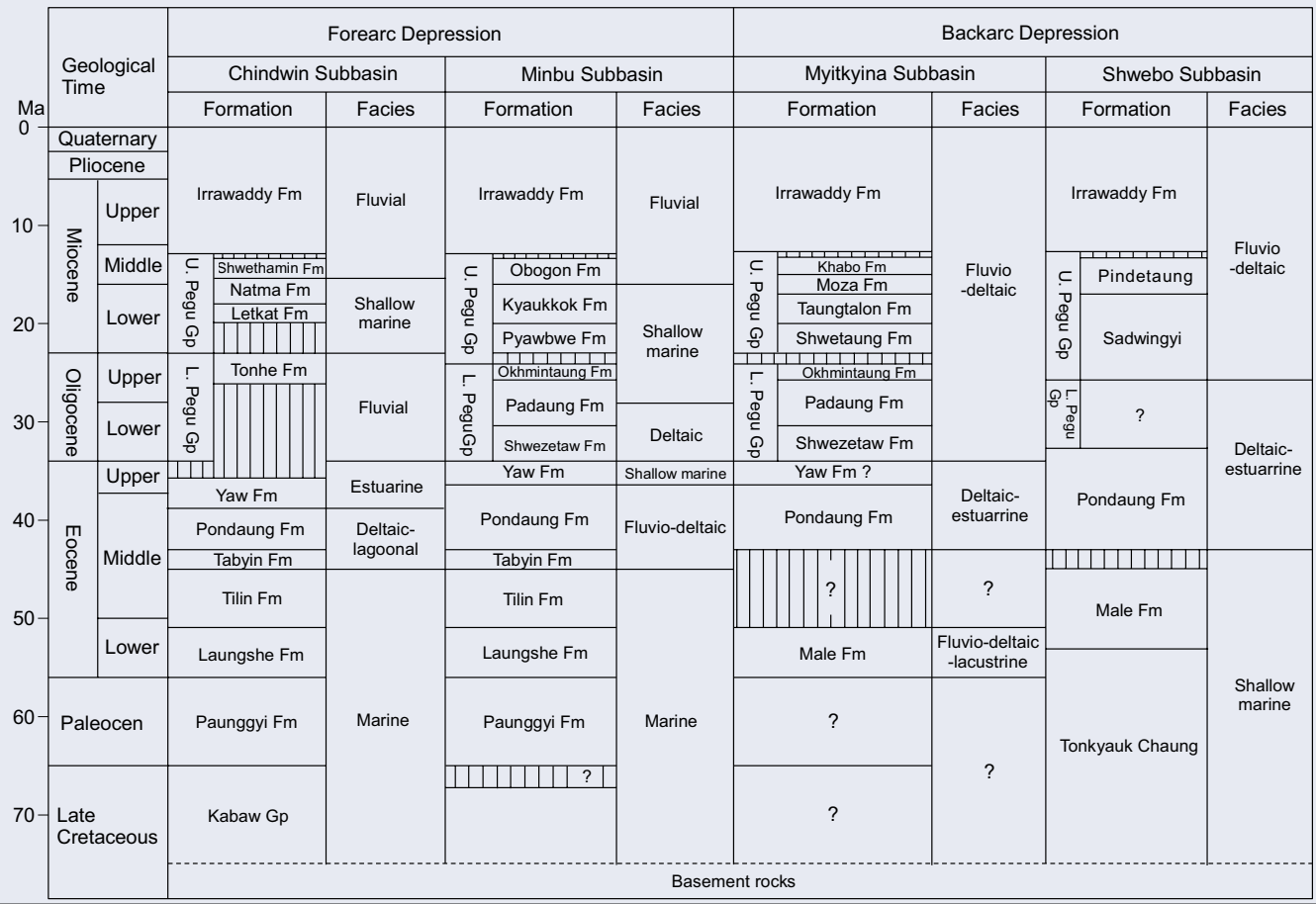

Note. Information taken From Licht et al. (2013, 2018), Arboit et al. (2021), Bender (1983), Htut (2017), and Zhang et al. (2021) and References therein.

In the forearc, marine facies predominate from Albian to middle Eocene times in both north and south sub-basins, becoming fluvio-deltaic to continental in the overlying Pondaung Formation. However, from the time of deposition of the Yaw Formation at the middle-late Eocene boundary (Licht et al., 2018), Licht et al. (2018) record divergence; the Yaw Formation in the Minbu Basin is exclusively shallow marine, while in the Chindwin Basin it is both marine and continental. Above the Yaw formation there is an unconformity in the Chindwin Basin but not in the Minbu Basin where sedimentation continued with the deposition of the Oligocene Shwezetaw, Padaung and Okhmintaung Formation. The Chindwin Basin records fluvial facies from late Oligocene times onward, while mixed shallow marine and deltaic facies persist in the Oligocene in the Minbu Basin, passing up to fluvio-deltaic facies in the early Miocene, with fluvial facies beginning in the late middle Miocene to Pliocene. In the Chindwin Basin, Westerweel et al. (2020) diverges from Licht et al. (2018) by further dividing the Letkat Formation into the upper Oligocene Tonhe Formation and overlying lower Miocene Letkat Formation, divided by an unconformity of earliest Miocene duration. Backarc facies changes are approximately coeval to those of the forearc, where known. Table 1 illustrates the basin stratigraphy in detail.

2.2. Previous Work on the Provenance History of the CMB

Previous work on the CMB has focused on zircon U-Pb analyses to allow discrimination between Mesozoic-Cenozoic arc-derived grains versus older crustal input (Cai et al., 2020; Licht et al., 2018). Hf-isotope characterization of these Mesozoic-Cenozoic grains allows for discrimination between zircons from the WPA, which have positive εHf values, as opposed to grains of similar age from the MMB, which have negative values (Wang et al., 2014). Other techniques have included rutile U-Pb analyses, with Cenozoic grains interpreted

as derived from the MMB (Zhang et al., 2021), and rutile geochemistry to assess metamorphic grade (Arboit et al., 2021). Arboit et al. (2021) also applied U-Pb thermochronology to titanite and apatite, the latter also including trace element geochemistry, to determine the source region's timing of cooling and grade of metamorphism. Sr-Nd bulk analyses (Licht et al., 2013, 2014) documented changing proportions of arc versus crustal material through time, and petrographic data have also been used to assess changes in the source region (Cai et al., 2020; Licht et al., 2013, 2014; Wang et al., 2014).

The overwhelming predominance of Mesozoic and Cenozoic zircons with positive εHf values in the Paleocene-middle Eocene sediments is interpreted by most researchers to indicate major input from the WPA and its proposed continuation in the now subducted or otherwise removed Greater Burma terrane to the north (Cai et al., 2020; Wang et al., 2014). The thickness of Eocene detritus in the CMB (e.g., Zhang et al., 2021) may indicate that the removed component of the Greater Burma terrane was quite substantial. Some samples with a significant component of older grains presumably indicate input from Burmese basement such as the Kampetlets schists and Pang Chaung turbidites. Arboit et al. (2021) additionally suggest the possibility of some Himalayan input, delivered by the Bengal Fan/longshore drift.

For formations younger than middle Eocene, provenance is debated. Old zircons and metamorphic lithic fragments in the uppermost middle to lowermost upper Eocene Yaw Formation are considered by Westerweel et al. (2020) and Morley et al. (2021) to be derived from within the WBT, such as either the Naga metamorphic rocks (Aitchison et al., 2019) or the now-subducted Greater Burma to the north. Westerweel et al. (2020) consider that this provenance continues to be dominant in the upper Oligocene Tonhe Formation, with first input from the MMB in the lower Miocene Letkat Formation. In this scenario, contact between Sibumasu and the WBT is not required until the Miocene. By contrast, Zhang et al. (2021) considered that MMB detritus first reached the CMB sometime between the late Eocene and the middle Oligocene, as also proposed by Arboit et al. (2021), while Licht et al. (2018) consider the first appearance of MMB detritus to be in the uppermost middle Eocene to lowermost upper Eocene Yaw Formation, thus requiring contact between Sibumasu and the WBT by the Oligocene and Eocene, respectively.

2.3. Previous Work on the Exhumation History of the IBR

An early IBR exhumational phase, in the Cretaceous, has been proposed based on the presence of unconformities of that age in the region (e.g., Brunnschweiler, 1966; Mitchell et al., 2010), evidence of schist and ophiolitic clasts from the IBR core in Cretaceous IBR sedimentary rocks (e.g., Morley et al., 2020; Rangin et al., 2013), and geochronological dating of rodingites (Liu et al., 2016) and the metamorphic sole of the accretionary prism (J. Zhang et al., 2017). Sedimentological observations, such as the facies change from Cretaceous-Eocene turbidites to imprecisely dated upper Eocene to Oligocene continental deposits in the IBR (Aitchison et al., 2019; Bannert et al., 2012; Ghose et al., 2014; Morley et al., 2020) also provide some constraint on the timing of exhumation of the accretionary prism. More precise timings of the exhumation of the IBR have been determined using two approaches: (a) interpretations of the provenance changes in the CMB described above in terms of changing paleogeography, and (b) low temperature thermochronology age elevation profiles in the IBR.

2.3.1. Changes in the CMB Interpreted in Terms of Exhumation of the IBR

Licht et al. (2018) documented a facies change from delta flood plain to a semienclosed barrier setting between the middle Eocene Pondaung Formation and the uppermost middle Eocene to upper Eocene Yaw Formation. They interpreted these changes as due to uplift of the nascent IBR, which formed a barrier. Arboit et al. (2021) noted a provenance change at ∼39 Ma, which they ascribed to decreasing proportions of Himalayan-derived (arc) material delivered to the CMB from the trench side to the west due to the uplifting IBR acting as a barrier. Zhang et al. (2021) and references therein, recorded a change in provenance sometime between late Eocene and middle Oligocene times in the CMB. They interpreted this provenance change to represent a shift from local derivation from the WPA to input from the MMB to the north. They concluded that, by this time, the Ayeyawady River must have been in evidence to transport material from the north, requiring an uplifted IBR as its western valley side. However, due to lack of samples over the intervening late Eocene to early Oligocene period, the time of change could not be tied down more precisely.

2.3.2. Exhumation of the IBR Determined From Three Age Elevation Profiles, Coupled With Provenance Data From East and West of the IBR

Najman et al. (2020) published the only age elevation transect on the IBR, to date. These profiles, in the Mindat region, at the latitude of the paleohigh separating the Minbu and Chindwin sub-basins, showed: (a) a significant period of exhumation around the Oligo-Miocene boundary in the IBR core (19–23 Ma; slightly earlier once advection is taken into account); (b) a period of exhumation to the east in the Kabaw Fault zone at 28–32 Ma (early Oligocene) but with large analytical uncertainties, and (c) tentatively, a possible earlier period of exhumation at or prior to 40 Ma (middle Eocene) in the IBR core, for which further work is required to confirm or refute. In the same paper (Najman et al., 2020), the age elevation profile was coupled with provenance data from the adjacent CMB. These data broadly showed (i.e., averaging between sub-basins with different geological histories after they were partitioned from ∼39 Ma (Licht et al., 2018)), that until at least the middle Eocene (48–38 Ma), sediment from both east and west of the IBR was derived predominantly from the Wuntho-Popa magmatic arc to the east. This indicates that the IBR had not formed a barrier sufficiently developed to impede westward transport by this time.

3. Strategy and Methods

As summarized in Section 2.2, we (Zhang et al., 2021) previously presented evidence for a change in provenance as occurring definitively sometime after the late middle Eocene and by the middle Oligocene. Therefore, we focused our new analyses on upper Eocene and lower Oligocene forearc basin sediments to more precisely constrain the time of provenance change, and we also incorporated new data as referenced in the appropriate figure captions.

Additionally, our previous work using rutile U-Pb analyses (Zhang et al., 2021) had assumed that grains with Cenozoic U-Pb ages were derived from the MMB. In our current paper, we therefore first undertook rutile analyses from the Ayeyawady headwaters that drain the MMB to confirm this interpretation.

We undertook a second age elevation transect (Tedim transect) to determine how regionally applicable our first transect was (Najman et al., 2020). Our new transect lies ∼200 km north of our previous transect at Mindat (Figure 1). The location was chosen because it allowed for the collection of multiple steep profiles within fault blocks that are comparable with the previous work. We also undertook additional low temperature thermochronological analyses and modeling of our previous Mindat transect in order to better compare the two transects.

Sample locations are given in SI 1, and detailed methodological descriptions are provided in SI 2, with summaries given below.

3.1. Petrography

450 points were counted on 10 sandstone samples from the CMB using the Gazzi-Dickinson method (Ingersoll et al., 1984). Sandstone classification was based on the relative abundance of the three main framework components quartz (Q), feldspars (F), and lithic fragments (L), considered if exceeding 10%QFL (e.g., in a litho-feldspatho-quartzose sand Q > F > L > 10%QFL; classification scheme after Garzanti, 2019). Full quantitative information was collected on rock fragments, classified according to protolith composition and metamorphic rank (Garzanti & Vezzoli, 2003). Median grain size was determined in thin section by ranking and visual comparison with sieved in-house standards.

3.2. Isotopic Analyses

Sr and Nd isotopes on bulk mudstones (six samples from the CMB), together with laser ablation U-Pb analysis of zircon (eight samples, six from the CMB and two from the IBR) and rutile (eight samples, four from the CMB, one from the IBR and three modern river sands), and Hf-isotope analysis of zircon (six samples from the CMB), were carried out at the Geochronology and Tracers Facility, British Geological Survey, UK.

Bulk rock powders were leached in dilute acetic acid to remove carbonate material prior to dissolution. Sr and Nd were separated using AG50x8 and LN Spec resins, and analyzed on a Thermo Scientific Triton thermal ionization mass spectrometer operating in multi-dynamic mode.

U-Pb zircon analyses were carried out using a multicollector Nu Plasma HR mass spectrometer coupled to a New Wave 193SS solid state laser, using the 91,500 reference material (Wiedenbeck et al., 1995) as primary reference material. Plešovice zircon (Sláma et al., 2008) and GJ1 (using values recommended by Horstwood et al., 2016) were used as secondary references. Rutile U-Pb analysis was carried out with the same instrumentation using Sugluk (Bracciali et al., 2013), R10 (Luvizotto et al., 2009) and R19 (Zack et al., 2011) as reference materials. Rutile ages are corrected for common Pb (see Supplementary file for details). U-Pb data were reduced using Iolite versions 3 and 4 (Paton et al., 2011) and plotted using IsoplotR (Vermeesch, 2018). For grains >1,200 Ma in age, $^{207}Pb/^{206}Pb$ ages were used, with a discordance limit of ±10%. For grains <1,200 Ma, $^{206}Pb/^{238}U$ ages were used, with a discordance limit of ±5%.

3.3. Thermochronological Analyses

Thermochronological data were obtained from 17 IBR samples along the road passing through Tedim (Figures 1 and 2a). Five zircon fission track (ZFT) samples were dated at the University of Sao Paulo using the external detector method. Methodology followed Parra et al. (2009). Seventeen zircon and three apatite samples were analyzed using the (U-Th-Sm/He) (ZHe and AHe, respectively) methods at Universitaet Potsdam (alphachron) and GFZ-Potsdam (ICP-MS) following the methodology of Galetto et al. (2021) and Zhou et al. (2017). Eleven apatite fission track (AFT) samples were analyzed at the Universitaet Potsdam by ERS using the external detector method following the methods outlined in Sobel and Strecker (2003). Detailed methodological descriptions are provided in SI 2. AFT and ZFT ages are reported with 1 sigma errors (SI 3a, 3c); AHe and ZHe ages are reported with 1 standard deviation errors (SI 3b).

4. Results

4.1. Thermochronologic Age Patterns Determined by QTQt Modeling

We obtained thermochronologic ages using up to four methods per sample, with closure temperatures ranging over >170°C (e.g., Reiners & Brandon, 2006). A summary of the data is given in Table 2 and detailed data sets are provides in SI 3a, b and c. All ZFT samples have at least 1 population which is older than the sample depositional age, suggesting that the samples have not been heated significantly within the zircon partial annealing zone (ZPAZ; <~230°C–350°C; Reiners & Brandon, 2006). Therefore, we interpret these ages to represent partially reset (at least one population younger than depositional age) or unreset (all populations older than depositional age) detrital ages. Reset ZHe ages are interpreted to reflect in situ cooling through the zircon partial retention zone (ZPRZ; 140°C to ~220°C; Guenthner et al., 2013); partially reset samples only attained temperatures in the lower part of this range. All AFT ages are much younger than depositional age and therefore are interpreted to reflect relatively rapid cooling through the apatite closure temperature of ~120°C within the past ~10 Ma (e.g., Reiners & Brandon, 2006). All AHe ages are interpreted to reflect relatively rapid cooling through the apatite partial retention zone (APRZ; 40°C to ~80°C e.g., Reiners & Brandon, 2006). We performed inverse modeling with the QTQt program (v. 5.7.0), which uses a Bayesian transdimensional statistical approach to extract the most probable thermal history from robust data sets (Gallagher, 2012). Detailed descriptions of the modeling strategy and of each model are provided in SI 4; supporting figures are shown in SI 5.

4.1.1. Tedim Transect

The thermochronologic ages and sample elevations are plotted versus the position along the Tedim cross section within a topographic swath profile and on a geological map (Figure 2). We divided the Tedim cross section into five fault-bounded segments, named zones T1 to T5, from west to east. These blocks are separated by the Lemyo, Thoubal, Zunki and Kheng faults (Mitchell, 2018; Morley et al., 2020; Singh et al., 2016). The Lemyo Fault may be correlated with the Lelon Fault (Mitchell, 2018). In order to assess the thermochronologic data from each fault block together, we performed inverse modeling of each Tedim zone (Figure 3).

4.1.1.1. Zone T5 (Kheng Transpressive Shear Zone)

The three modeled samples from zone T5 (MY19-87a, -88a, -89a) were near the surface at a time corresponding to a late Triassic —early Jurassic depositional age (Yao et al., 2017). They were again near the surface between 127 and 115 Ma, when ophiolites were formed and emplaced (Liu et al., 2016). Subsequently, samples were heated by burial beneath sediments prior to final Cenozoic exhumation. Sample MY18-86a was not modeled due

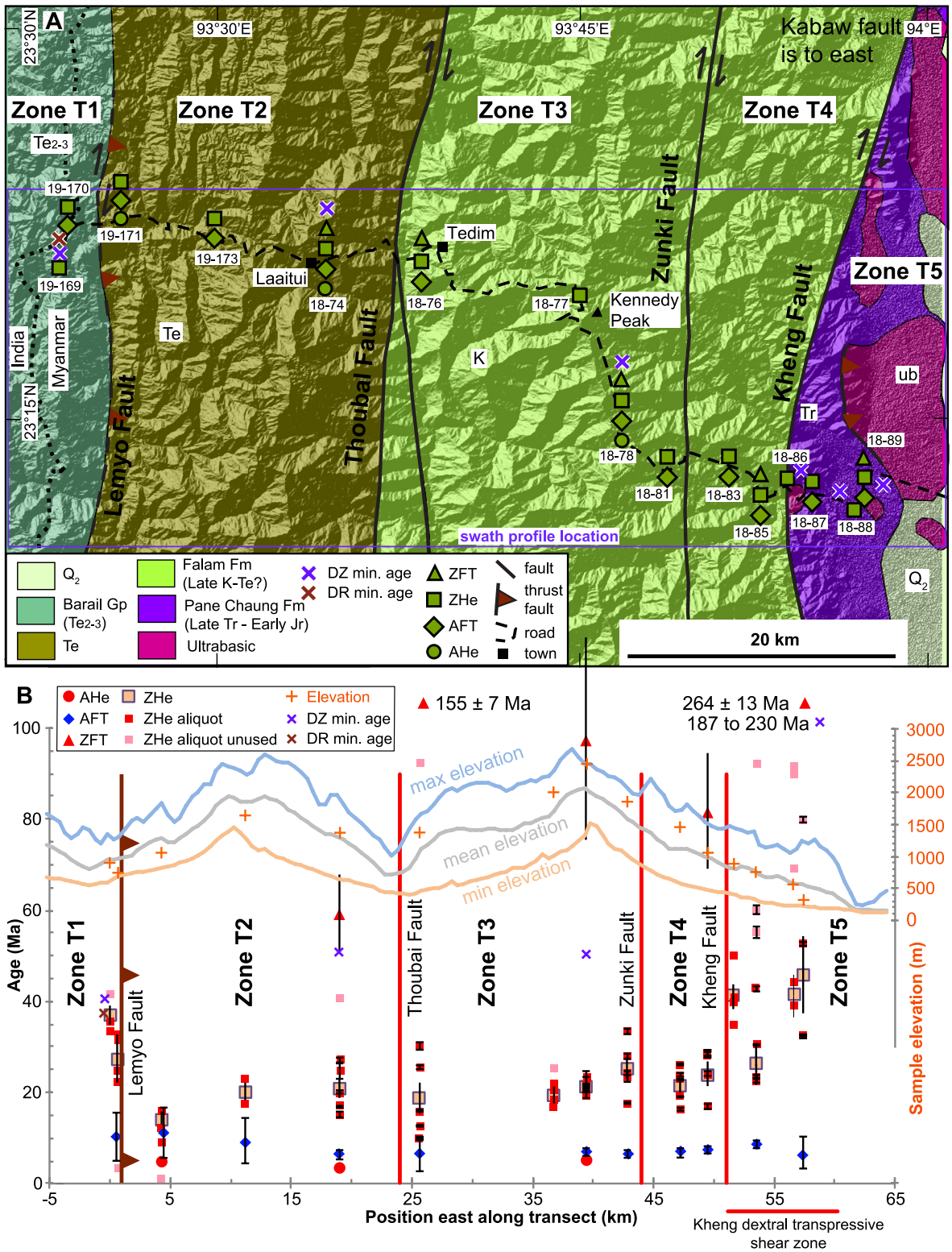

Figure 2. Tedim transect thermochronologic data displayed on a geologic map (a) and cross section. Geological map modified from Burma Earth Sciences Research Division (1977), Mitchell (2018), Morley et al. (2020), and Singh et al. (2016). Blue rectangle delineates footprint of topographic swath profile used to calculate minimum, mean and maximum elevations shown in (b). (b) Age (left axis) and elevation (right axis) of thermochronologic samples projected onto an east-west profile. Positions are shown with respect to the westernmost sample, MY19-169. Prefix MY- has been removed from sample numbers for clarity. Detrital zircon data in zone T5 is from Yao et al. (2017).

Tectonics

10.1029/2021TC007057

Table 2
Thermochronologic Data Summary

sample no.	Depo age	Elev (m)	km *E* of MY19-169a	Model zone	AHe age	St dev	Aliquots total/ used	AFT pooled age	1 s error	n	*P* (chi^2) %	ZHe age	St dev	Aliquots used for age	Age calculation	ZFT central age	1 s error	*n*	*P* (chi^2) %
Tedim vertical profile																			
74a	Te	1,369	19	T2	*3.4*	0.4	5 of 5	6.3	1.0	13	96	16.5	2.5	3 of 6	wm	59.5	4.0	20	72.3
76a	K	1,368	25.7	Not modeled				6.6	3.9	3	32	*18.8*	8.7	5 of 6	wm	164.5	21.6	20	0
77a	K	2,011	36.8	T3								19.4	1.8	4 of 5	rp				
78a	K	2,450	39.4	T3	5.7	0.2	1 of 1	6.9	0.9	22	95	21.4	1.5	6 of 6	wm	97.6	10.6	20	0
81a	K	1,861	42.8	T3				6.4	0.8	24	73	*21.4*	4.3	4 of 5	wm				
83a	K	1,464	47.2	T4				6.8	1.1	20	94	21.6	3.9	5 of 5	wm				
85a	K	1,048	49.5	T4				7.4	0.8	21	97	*24.0*	5.5	4 of 4	rp	81.8	6.1	20	0
86a	K	891	51.6	Not modeled								41.0	6.4	4 of 5	rp				
87a	Tr	759	53.5	T5				8.5	0.8	20	88	26.3	4.4	3 of 7	wm				
88a	Tr	566	56.6	T5								41.4	3.6	2 of 5	wm				
89a	Tr	313	57.4	T5				13.0	1.5	26	11	32.5	0.1	2 of 5	wm	285.3	31.2	20	0
169a	$Pg_{23}b$	898	0	T1								36.9	4.2	3 of 3	wm				
170a	$Pg_{23}b$	733	0.6	T1				10.6	1.1	20.0	11.0	28.0	5.2	4 of 5	wm				
171a	Te	1,055	4.3	T2	5.2	0.5	4 of 5	11.1	0.9	25.0	4.6	14.3	2.5	2 of 5	wm				
173a	Te	1,642	11.2	T2				9.7	1.2	19.0	65.0	20.2	4.0	2 of 3	wm				
Mindat profile-new data																			
17a	Tr	2,374										35.9	4.8	3 of 4	wm				
32a	Tr	2,103										27.4	4.2	4 of 5	wm				

Note. ZHe ages calculated using radial plots (rp) and weighted means (wm) in IsoplotR (Vermeesch, 2018). We report standard deviation of the ages of the individual aliquots used as a measure of the dispersion. Reported He ages are considered ages to be reproducible because the 1σ S.D. is <20% of the mean age except ages in italics. Depositional ages: $Pg_{23}b$, Eocene-Oligocene; Te, Paleogene; K, Cretaceous; Tr, Triassic. Aliquots used does not include 3 crystals that were discarded due to analytical problems. Sample numbers listed without prefixes MY16, MY18, MY19.

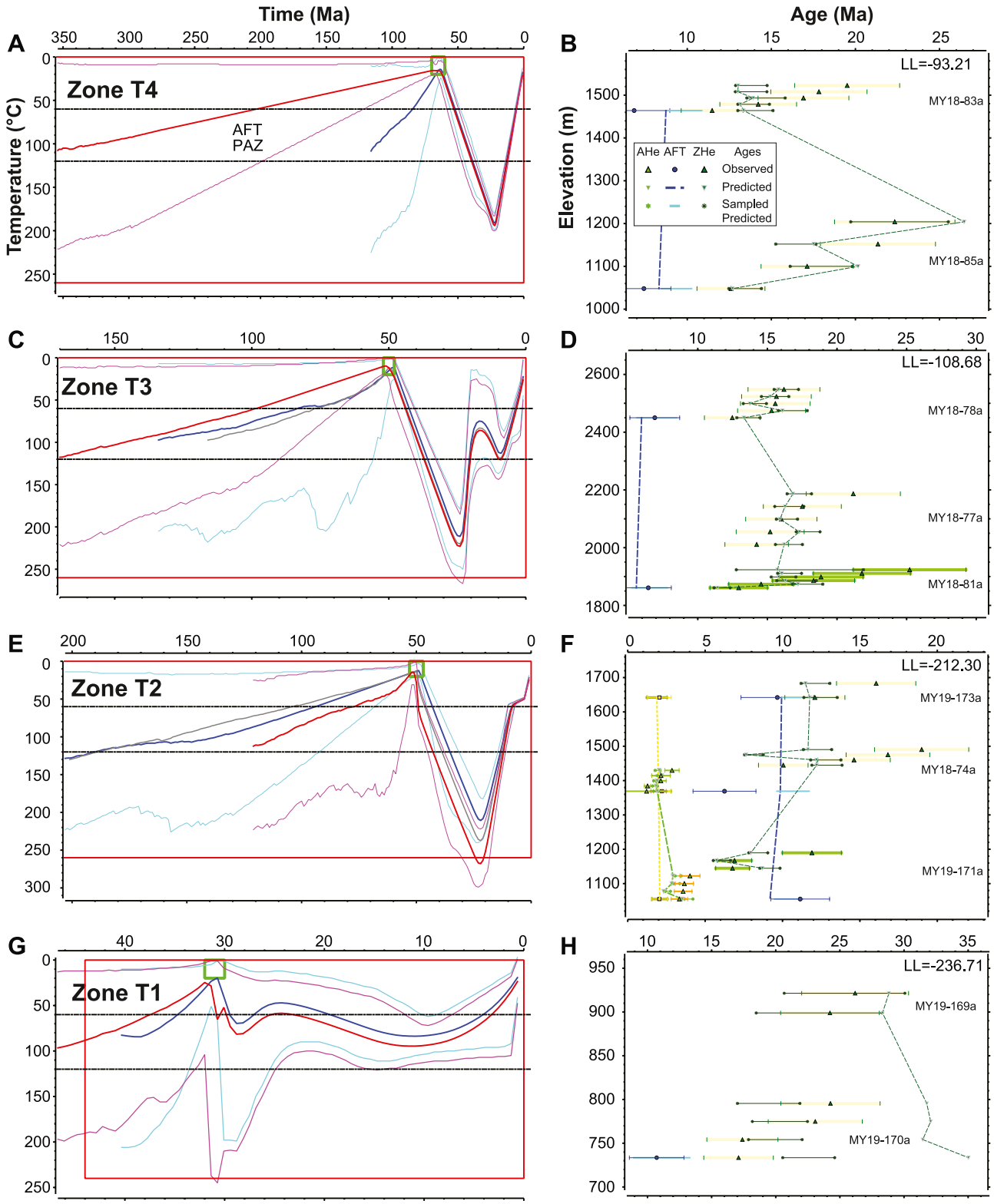
Time (Ma)
Age (Ma)
A
Zone T4
AFT
PAZ
Temperature (°C)
B
LL=-93.21
MY18-83a
MY18-85a
Elevation (m)
AHe AFT ZHe Ages
Observed
Predicted
Sampled
Predicted
C
Zone T3
D
LL=-108.68
MY18-78a
MY18-77a
MY18-81a
E
Zone T2
F
LL=-212.30
MY19-173a
MY18-74a
MY19-171a
G
Zone T1
H
LL=-236.71
MY19-169a
MY19-170a

Figure 3.

to ambiguity about its position with respect to the Kheng fault. The modeled ZHe samples all have significant age dispersion, which cannot be simply related to either eU or grain size (SI 5a). The likely explanation for the large ZHe age dispersal is variable inherited radiation damage; the zircons in this section have U/Pb ages ranging from 187 to ~1,200 Ma and older (Yao et al., 2017). An alternative possibility is that the ZHe crystals are not fully reset.

We tried two modeling strategies (SI 4a). First, we modeled all ZHe aliquots; this led to geologically unrealistic results and poor fits to the individual aliquots (Figure SI 5c). We also modeled just the younger ZHe aliquots on the logic that it is more common for older ages to be erroneous (Figure SI 5c). However, comparing these two models, the onset of rapid cooling is clearly dependent on the choice of aliquots modeled and one could easily obtain different model results by selecting a different aliquot (SI 4a). Therefore, we refrain from using the model results from this zone.

4.1.1.2. Zone T4 (Kheng Fault to Zunki Fault)

The thermal model (Figure 3a) shows monotonic heating from late Cretaceous deposition (Mitchell et al., 2010) (Figure 2) to T_{max} of ~180°C–200°C at ~24–22 Ma followed by monotonic rapid cooling starting around 22 Ma (24–21 Ma).

4.1.1.3. Zone T3 (Between Zunki and Thoubal Faults)

The thermal model (Figure 3c) shows monotonic heating from the 45–49 Ma depositional age based on the MDA from sample MY18-78A determined from detrital zircon U-Pb data (SI 3d), to a T_{max} of ~180°C–260°C at ~25 Ma, followed immediately by 5–10 Myrs of rapid cooling. There is a possible reheating interval between ~18 and 10 Ma, then renewed rapid cooling beginning at ~10 Ma. The apparent reheating could reflect a combination of a decrease in the exhumation rate and advection rather than burial.

4.1.1.4. Zone T2 (Thoubal Fault to Lemyo West-Vergent Fault)

The thermal model (Figure 3e) shows monotonic heating from the ~50 Ma depositional age based on the youngest detrital zircon U-Pb age in MY18-74A (SI 3d), to a Tmax of ~170°C–300°C at ~21 Ma, followed immediately by rapid monotonic cooling. The cooling rate decreases between ~9 and ~3 Ma before increasing again.

4.1.1.5. Zone T1 (West of Lemyo West-Vergent Thrust)

Samples from Zone T1 were collected from the Eocene-Oligocene Barail Group (Handique et al., 1989) near the Indian border (Figure 2). The depositional age is constrained by sample MY19-169A, which has one discordant U/Pb zircon at ~40 Ma as well as three detrital rutiles between ~41 and 37.5 Ma (SI 3d and e). The same sample yielded three ZHe ages: 33.4 ± 0.6, 35.8 ± 0.4, and 41.6 ± 0.5 Ma. Zone T1 has a younger depositional age and a more distal position than zone T2 and therefore would be expected to have lower maximum burial temperature but a generally similar pattern of burial heating. Therefore, we interpret the zircon crystals to represent roughly syn-depositional volcanic grains which have only experienced enough burial to reset the AFT age of sample MY19-170A (Figure 3g). Alternatively, the ZHe ages could reflect Himalayan-derived detrital material, similar to results from sample 16CMP7, collected 25 km to the NW from the middle Barail Group (Betka et al., 2021); this scenario would require a similar magnitude of burial heating over a shorter interval. The thermal model shows a poorly constrained cooling path close to the deposition age, which is set to 32–30 Ma. The model then shows slow heating between ~25 and 15–10 Ma, followed by slow cooling beginning at ~13–10 Ma. Maximum burial temperatures were 80°C–120°C.

4.1.2. Mindat Transect

We modeled the cooling history of two of the three blocks from the Mindat transect using new ZHe data and data presented in Najman et al. (2020) in order to strengthen the conclusions of that study (Figure 4).

Figure 3. Tedim QTQt model results for zones T4 through T1. Left column (a, c, e, and g) shows the expected thermal history models. The red curves denote the "hot sample" and the dark blue curves the "cold sample" with their respective 95% confidence intervals. Heavy green boxes indicate the depositional age constraints. Red box delineates the model space. Right column (b, d, f, and h) shows how well the model fits the observed data; key is in panel (b). We present the values predicted for the expected thermal history model and the two-sigma interval of the data predicted by the post-burn-in acceptable models. For samples with multiple ZHe or AHe ages, a small elevation perturbation was added to the plot to facilitate data visualization. The predicted ages are connected by dashed lines. Note that the model fits shows AHe and ZHe Ft uncorrected ages. LL is Log-likelihood. Model results for zone T5 are shown in SI 5c.

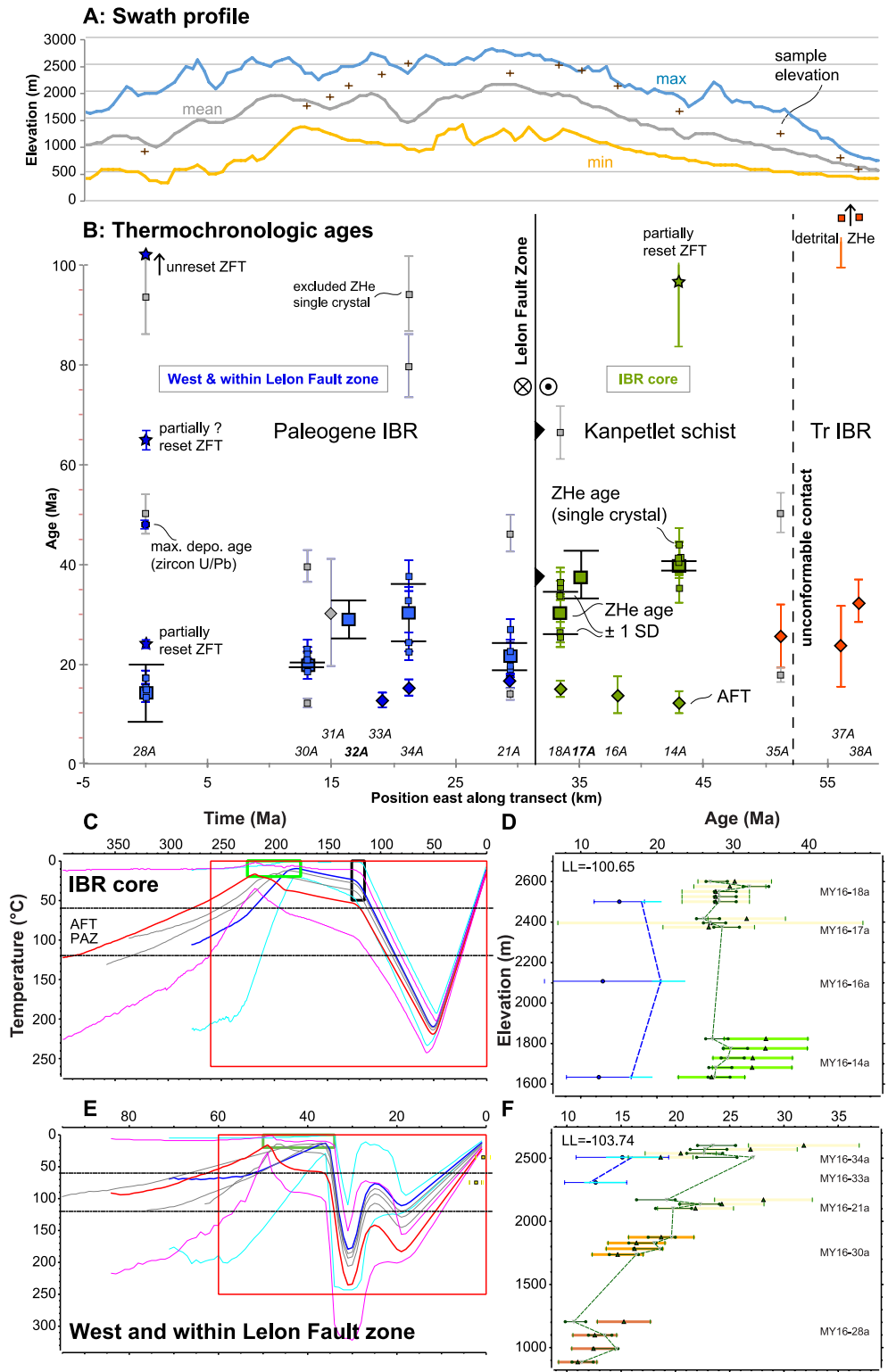

Figure 4. Mindat transect thermochronologic data. (a) Swath profile showing minimum, mean, and maximum elevations and sample locations. (b) Thermochronologic ages and detrital zircon maximum depositional ages projected onto an east-west profile. Sample numbers are shown without prefix MY16-for clarity. (a, b) are slightly modified from Najman et al. (2020); this reference also provides a geological map of the transect. (c, e) QTQt expected thermal history models of the IBR core and the area west and within the Lelon fault zone, respectively. (d, f) Model fits to the observed data. Figure explanations and the symbols used are the same as in Figure 3.

4.1.2.1. Mindat IBR Core

The Mindat IBR core profile includes data from four samples: one unreset or partially reset ZFT age, three ZHe samples with a total of 11 reproducible aliquots, and three AFT samples (Figure 4b). Here, we neglect three younger ZFT crystals that have too much age dispersion to define a single population. The new ZHe data from sample MY16-17A are reported in Table 2 and SI 3b. In addition, sample MY16-35a likely belongs to this profile. As this sample has one low resolution AFT age, two discordant ZHe ages, and a partially reset ZFT age, it was not included in the thermal model. Recent mapping suggests that the Kanpetlet schist is bounded to the east by an unconformity (Morley et al., 2020) rather than by the Kabaw fault, as portrayed in Najman et al. (2020); therefore, we have modified the cross section shown in Figure 4b. The model (Figure 4c) shows that the profile was near the surface at the Triassic depositional age (Yao et al., 2017) and again around ~128–115 Ma, when ophiolites were formed and emplaced (P. Zhang et al., 2017). Subsequently, samples were heated by burial beneath sediments until ~57–49 Ma and ~200–240°C. Monotonic cooling commenced at ~49 ± 3 Ma and continued until the present. This fault block is correlated with zone T5 of the Tedim profile.

4.1.2.2. West of and Within the Lelon Fault Zone

The QTQt model for the western end of the Mindat profile (west and within Lelon fault zone; Figures 4b and 4f) includes data from five samples: one partially reset ZFT age, four ZHe samples with a total of 23 aliquots (of which five were discarded), and two AFT samples. The new ZHe data from sample MY16-32A are reported in Table 2 and SI 3b; the remaining data are from Najman et al. (2020). The ZHe data generally show a good age-elevation trend (Figure 4f). The thermal model shows a complex pattern, with rapid post-depositional heating to 310°C–150°C at ~30 Ma, followed by a pulse of cooling until 27–22 Ma, then reheating until ~19 Ma, and finally monotonic cooling. The apparent reheating could reflect a combination of a decrease in the exhumation rate and advection rather than burial.

4.1.3. Summary of Thermochronologic Results

In zones T2, T3, and T4 of the Tedim profile, and the Mindat IBR core, ZHe ages young westward within each block. Not all of the ages are correlated with elevation. Two of the three samples in Zone T5 of the Tedim profile also follow this pattern. In addition, the QTQt models show a very small thermal offset between the lowest (hot) and highest (cold) samples. However, the elevation offset between the samples would suggest a larger thermal offset. This pattern could be explained by rotation of the blocks about a horizontal axis trending subparallel with the bounding fault systems. This may be caused by west-vergent thrusting on the western-margins of the fault blocks or possibly by deformation within the individual blocks.

Our QTQt modeling shows that most of the ranges covered by our transects have experienced over 160°C of Cenozoic exhumation. The core of the range, exposing Triassic strata and metamorphic rocks, commenced a period of exhumation in the early-middle Eocene. This is slightly earlier than the poorly dated change from deep marine to continental facies between the middle and late Eocene in the IBR (cf. Sections 2.1.2 and 2.3). The bulk of the exhumation initiated in the latest Oligocene and propagated westward. The AFT ages are quite consistent across much of the range, with most ages between 6 and 9 Ma, irrespective of elevation. This could suggest that the range has reached an exhumational steady state (e.g., Reiners & Brandon, 2006). In contrast, AFT ages in the far western region are slightly older (6–11 Ma), reflecting the slower exhumation in this block (Figure 3).

4.2. Provenance Data

In summarizing the salient points of our results, we put them in context of previously published results.

4.2.1. Petrography

The analyzed samples (reported in data set SI 3g and graphically presented in Figure SI 6) range from very-fine to medium sand ($4.0 - 1.4\ \phi$). The majority of samples of late Eocene (Chindwin Basin) or Early Oligocene (Minbu Basin) ages and younger are litho-feldspatho-quartzose. Samples older than late Eocene have more feldspar and/or lithic fragments in both basins. An evolutionary trend from the middle Eocene to the Miocene is documented by increasing sedimentary and metamorphic lithic fragments, at the expense of volcanic lithic fragments. Petrography is stable from Miocene onward.

In the Chindwin Basin, the feldspar-rich middle Eocene Pondaung Formation indicates predominant derivation from the roots of a magmatic arc. The major influx of metamorphic detritus is indicated by biotite and staurolite in the lower Miocene Letkat Formation, indicating supply from amphibolite-facies metasedimentary rocks. The underlying latest middle to lowermost upper Eocene Yaw Formation is transitional between the Pondaung and Letkat formations. Oligocene rocks were not sampled in the Chindwin Basin. The onset of metamorphic detritus is more difficult to pin-point in the Minbu Basin. Eocene to Lower Oligocene sandstones of the Pondaung and Shwezetaw Formations are volcaniclastic and chiefly arc-derived. The most significant petrographic change is marked by decreasing plagioclase and volcanic detritus, which are largely arc-derived, with a relative increase in quartz, *K*-feldspar and amphibole. This provenance change occurs between the lower Oligocene Shwezetaw Formation and the upper Oligocene Okhmintaung Formation, with the occurrence of amphibole at this time suggesting input from amphibolite-facies metamorphic rocks rather than the arc (Andò et al., 2014). Biotite becomes abundant and staurolite common in lower Miocene sandstones which also contain garnet, while kyanite is first recorded in the Irrawaddy Formation above. This indicates that supply from amphibolite-facies metamorphic rocks continued throughout the Neogene.

4.2.2. Zircon U-Pb With Hf (Data Set SI 3d)

As illustrated in Figure 5, previous data from all CMB sub-basins studied (Chindwin and backarc/on-arc) show that for all formations up to and including middle Eocene strata, the <250 Ma zircon population has almost exclusively positive εHf values (Arboit et al., 2021; Lin et al., 2019; Wang et al., 2014). We now show that this is also true for the Minbu Basin (sample MY16-05A, middle Eocene).

No previously published data are available for the latest middle to lowermost upper Eocene Yaw Formation. The only available data were from the upper Eocene backarc sediments (Zhang et al., 2021), which show a predominance of grains with positive εHf values for grains <250 Ma, but with a low number of analyses. Our new data from the Yaw Formation (MY18-95A) show that Mesozoic-Cenozoic zircons with negative εHf values remained rare in the CMB during this time interval.

Above the Eocene, there were previously no published data from the forearc strata until the Miocene (Arboit et al., 2021; Wang et al., 2014), where detrital zircons in the <250 Ma age range have an appreciable proportion of grains with negative εHf values. Our new data from the Minbu forearc sub-basin show that all <250 Ma zircons have positive εHf values in the Lower Oligocene sample (MY16-06A). Grains with negative εHf values first appear in this basin in the Late Oligocene. This is similar to published data from the backarc/on-arc succession that showed the first significant input of zircons with negative εHf values in middle Oligocene strata (Arboit et al., 2021; Robinson et al., 2014). In all basins studied, the proportion of grains with such a signature progressively increase into the Neogene.

4.2.3. Rutile U-Pb (Data Set SI 3e)

As illustrated in Figure 6, previously published data from all studied CMB sub-basins (Chindwin, Minbu and back-arc/on-arc; Arboit et al., 2021) show that formations up to and including the latest middle to lowermost upper Eocene Yaw Formation either have grain age spectra composed exclusively of ∼500 Ma and/or ∼100 Ma peaks, with no Cenozoic grains, or samples that contain no rutile. Cenozoic grains have been recorded from middle Oligocene (on arc/back arc basin) and lower Miocene (Chindwin Basin) strata and in these two basins no rocks from the intervening Eocene-Oligocene time periods have been available for study. Our new data from the Minbu Basin and modern Ayeyawady headwaters allow a more complete representation of the trend. The middle Eocene sample contains no rutile (MY16-05A) consistent with previous studies of this time period; the lower Oligocene sample (MY16-06A) contains a small Cenozoic population, which increases in dominance and youngest grains in the upper Oligocene sample (MY16-11A). This trend of increasing dominance of Cenozoic grains continues throughout the Neogene, also more clearly observed in our new data from Neogene samples including from the Chindwin Basin (MY16-10A—Lower Miocene, MY16 09 and 56A—middle Miocene-Pliocene).The present day modern Ayeyawady sands (upper Ayeyawady River; samples MD297, 298, 393) have somewhat lower percentages of Cenozoic grains compared to the Neogene strata.

4.2.4. Sr-Nd Bulk Rock (Data Set SI 3f)

Sr-Nd bulk data has previously been used in the CMB to assess the varying contributions of arc versus older continental crustal material through time. Utilizing data from both sandstone and mudstone, and reporting εNd

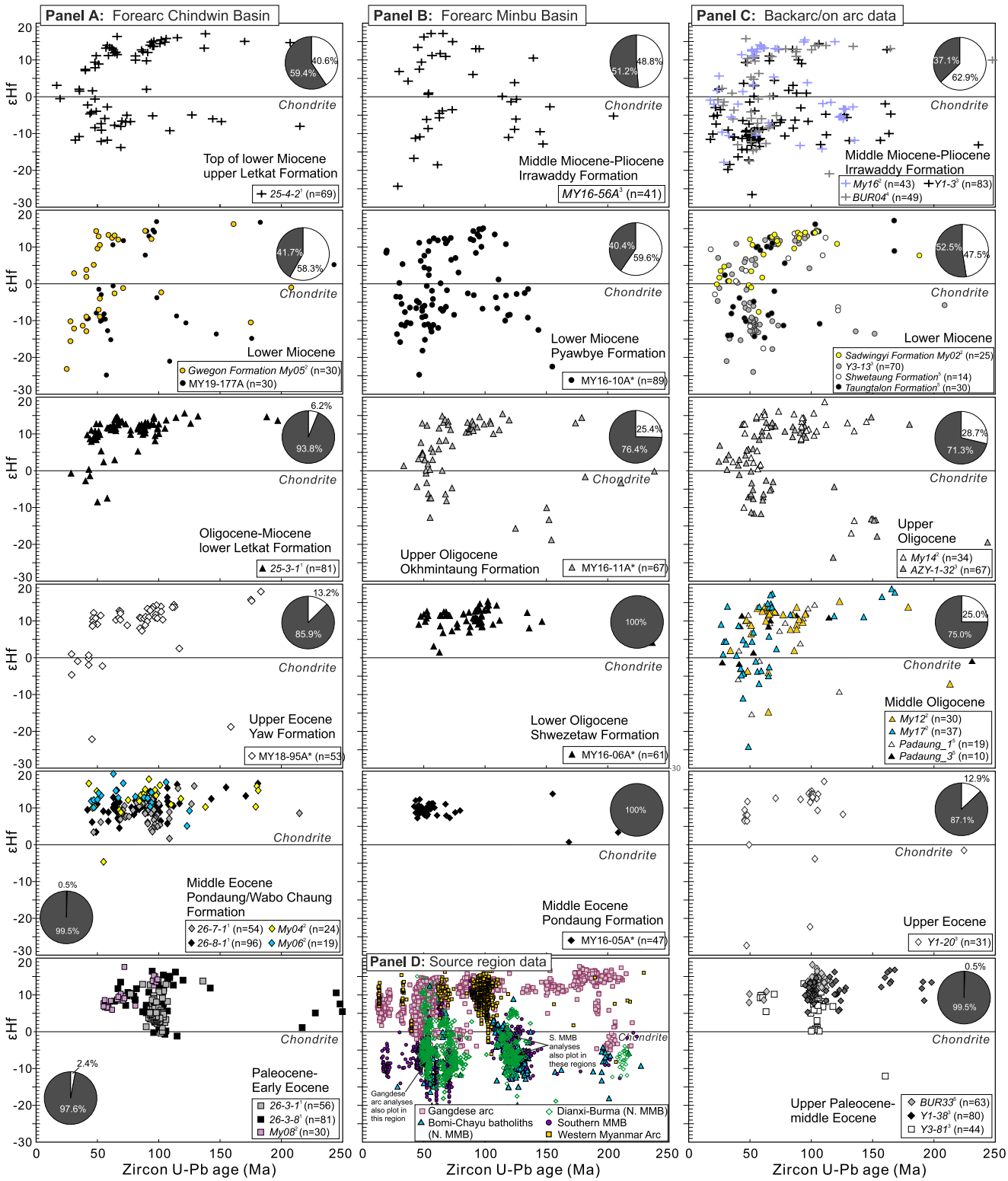

Figure 5. Zircon U-Pb with Hf data. Pie charts show the proportion of the <250 Ma zircon population which have positive (black) versus negative (white) εHf values. Samples marked with * are our new data. Published data: 1-Wang et al. (2014), 2-Arboit et al. (2021), 3-Zhang et al. (2021), 4-Liang et al. (2008), 5-Robinson et al. (2014), 6-Lin et al. (2019). Panel (d) taken from Zhang et al. (2021) and references therein, updated with data from Gardiner et al. (2018), Li et al. (2019, 2020), Lin et al. (2019) and Zhao et al. (2017).

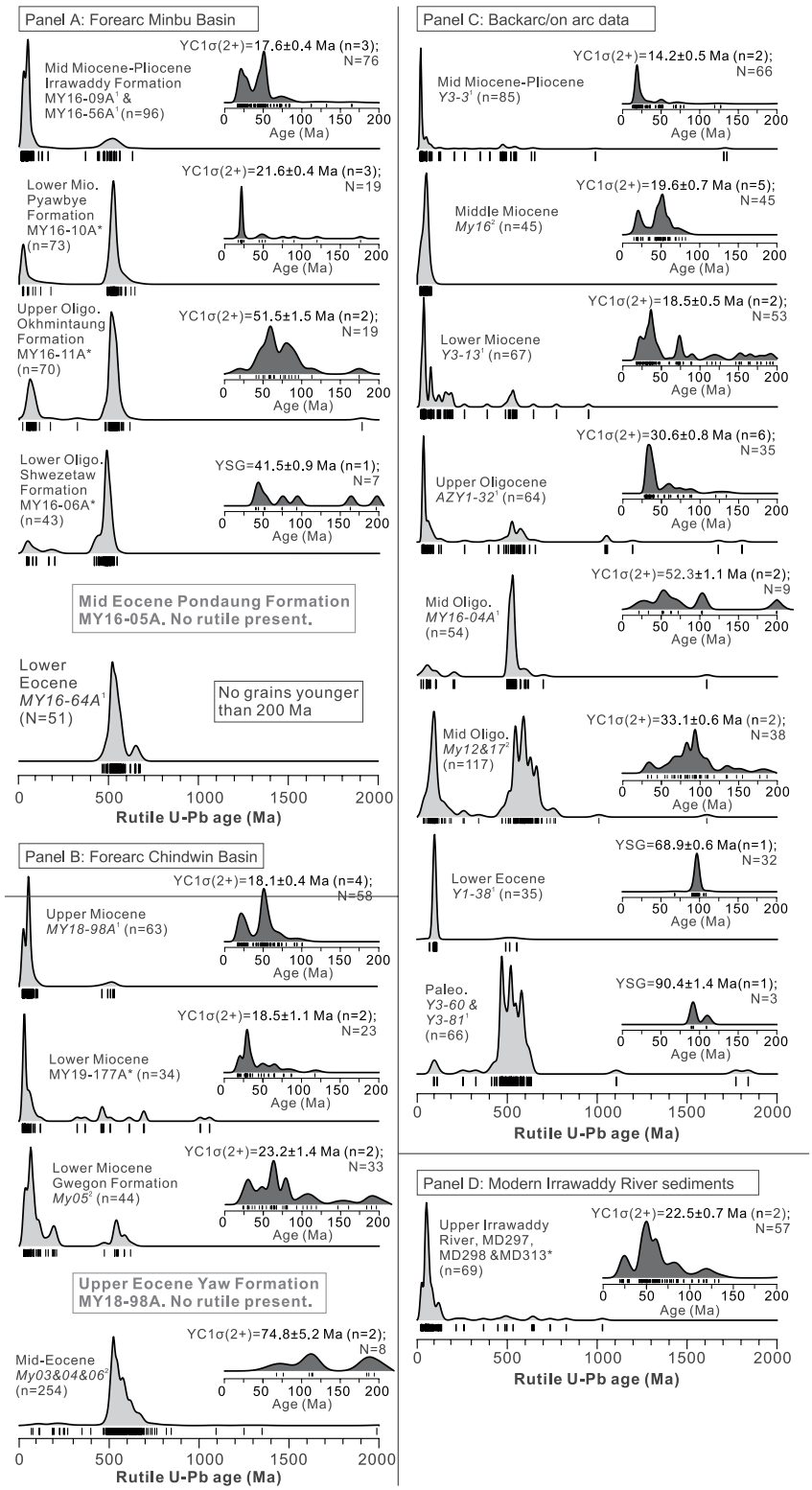

Figure 6. Rutile U-Pb data. Our new data are marked by asterisks, while the published samples are shown by numbers: 1-Zhang et al. (2021) and 2-Arboit et al. (2021).

values only, Licht et al. (2014) noted a trend to increasingly negative (crustal) values in the Minbu forearc basin from the start of their studied record in the middle Eocene Tabyin Formation, with values becoming stable by the Miocene. Later, Zhang et al. (2021) utilized paired $^{87}Sr/^{86}Sr$ and εNd values, and combined both the data from Licht et al. (2013) with their additional data from the Minbu forearc basin, as well as reporting the first data from the backarc.

We augment data summarized above from the forearc basin by adding new data from the Chindwin sub-basin, and additionally plotting the data of Licht et al. (2013) and Licht et al. (2014) as individual points. Note that we only plot their bulk mudstone or <2 micron fraction samples because their data shows appreciable difference between >163 and <2 micron grain-size fractions. The resulting Figure SI 7a shows the trend to increasing proportions of old continental crustal material through time as originally proposed by Licht et al. (2014). This trend begins at least by the middle Eocene, and there is no step change in the Yaw Formation, or discernible difference between the Yaw Formation and underlying middle Eocene Pondaung Formation. In the backarc basin, the data of Zhang et al. (2021) record increasing input of older continental crustal material beginning sometime after the middle or late Eocene and before the late Oligocene. We added a sample from the middle Oligocene (Figure SI 7b) and showed that the trend to increasing older continental crustal material had begun by this time.

5. Discussion

5.1. Provenance

As summarized in Section 2.2, different published provenance data sets have variously indicated a continuum of change since at least the middle Eocene (Licht et al., 2014), or a step change either in the uppermost middle to lowermost upper Eocene Yaw Formation (Licht et al., 2018), sometime between the late Eocene and early Oligocene (Zhang et al., 2021), or across both the middle Eocene-early Oligocene and Oligo-Miocene boundaries (Westerweel et al., 2020). Furthermore, the source of the detritus is also debated, with MMB material considered to have first arrived on the WBT either at the middle-late Eocene boundary as detected in the Yaw Formation (Licht et al., 2018), sometime between the late Eocene and middle Oligocene (Zhang et al., 2021), Oligocene (Arboit et al., 2021; Zhang et al., 2021), or Miocene (Westerweel et al., 2020). The timing of these provenance changes constrains when the WBT docked with Asian Sibumasu.

We are not confident that the Yaw Formation documents an abrupt change in provenance as argued by Licht et al. (2018), based on the first appearance of old zircon grains, because such grains have already appeared sporadically but in appreciable numbers in older strata (Figure SI 8—zircon U-Pb KDEs), as indeed noted by those authors as evidence of ephemeral earlier exhumation. Likewise, it should be noted that the petrographic change reported at the Pondaung-Yaw Formation boundary in the Chindwin Basin, with increasing metamorphic lithic fragments at the expense of volcanic lithics, also reflects a change in operator (data obtained by Wang et al. (2014) for the Pondaung Formation vs. data obtained by Licht et al. (2018) for the younger units). Petrographic data are sensitive to operator nuances, and in fact, when looking at the data collected by one operator only (Licht et al., 2018) their one datapoint for the "pre Yaw unit" (Paunggyi Fm) is similar to that of their Yaw data, with the main change occurring between the Yaw and the Letkat formations. This is similar to what we observe in our new data set (Figure SI 6), with the most significant change on an overall evolution from middle Eocene to Miocene times occurring at the latest Oligocene to Miocene times. Furthermore, Yaw Formation zircon Hf values (Figure 5) and Sr-Nd signatures (Figure SI 7) remain similar to those of the underlying Pondaung Formation.

Regardless of whether a change occurred in the Yaw Formation, the important issue is whether the nonvolcanic material reflects input from the MMB and therefore whether WBT-Sibumasu collision had occurred by that time. As previously proposed by Westerweel et al. (2020) and Morley et al. (2021), old zircons and metamorphic rock fragments may reflect greater contribution from Burmese basement where, e.g., Triassic schists show a significant pre-Devonian zircon population (Najman et al., 2020; Yao et al., 2017), and/or from the now-subducted Greater Burma region or Naga metamorphic rocks of the WBT. To this discussion, we bring the first zircon εHf data from the Yaw Formation, which shows a paucity of grains with negative values, indicating an absence of zircons from the MMB. We therefore concur with those previous workers who propose a source within the WBT for the nonvolcanic detritus deposited in the Yaw Formation of the CMB in latest middle to earliest late Eocene times.

Arboit et al. (2021) also note a change in provenance in the middle to late Eocene. They tentatively ascribe this provenance to Bengal Fan Himalayan detritus, delivered to the CMB from the west, with decreasing Himalayan input again from 39 Ma due to the uplifting IBR acting as a barrier. Their argument for a new Himalayan provenance in the middle-late Eocene can be summarized as follows: samples include Neoproterozoic-Cambrian zircons with Hf values as low as −50 which they suggest have not been so far recorded in the WBT; zircon Hf values of the Mesozoic-Cenozoic grains become more heterogenous compared to underlying formations; and apatite and titanite grains dated 110–85 Ma have geochemical compositions indicative of derivation from high grade metamorphic rocks suggested to be from the Lhasa terrane north of the Himalayan Yarlung-Tsangpo suture zone. However, we note the following: (a) the Pane Chaung Formation (Triassic turbidites of the IBR, thought to represent the unmetamorphosed equivalent of the Kanpetlet Schist of the Burmese basement (Bannert et al., 2012; Morley et al., 2020)) contain zircons of suitable age and εHf affinity (Yao et al., 2017); (b) εHf values do not become significantly more heterogenous; there is only one Mesozoic-Cenozoic zircon with negative εHf value, all others being of positive signature compatible with a WPA source; (c) the, albeit limited, studies of titanite from the Lhasa Block all have ages <100 Ma and the majority <85 Ma (Guo et al., 2020); (d) a Himalayan suture zone high-grade metamorphic source delivered to the CMB via the Bengal Remnant Ocean Basin and the Indian Ocean represents a paleodrainage pattern not easily envisioned both in terms of (a) the depositional patterns that would be required, and (b) the lack of high-grade metamorphic charnockite material recorded in petrographic data from late Eocene rocks of the Bengal (Surma) Basin (Najman et al., 2008); metamorphic minerals are not recorded in the Surma Basin until post-Eocene times (Bracciali et al., 2015).

Zhang et al. (2021) previously proposed a change in provenance sometime between the late Eocene and middle Oligocene. They noted the first appearance of zircons with negative εHf values typical of the MMB and Cenozoic rutiles, which they interpreted as MMB-derived, by the middle Oligocene. With our new data that better span the missing time interval, we now refine the change as occurring after the latest middle to lowermost upper Eocene Yaw Formation (depositional age ∼39–37.8 Ma Licht et al., 2018), as evidenced by the Mesozoic-Cenozoic zircons with positive εHf values, and by the early Oligocene, as evidenced by first appearance of Cenozoic rutile at this time. First input of MMB-derived material from the Asian plate in the later late Eocene or by the early Oligocene at latest, is coeval with the unconformity above the Yaw Formation, interpreted as due to collision of the WBT with Asia (Westerweel et al., 2020). Our interpretation of first MMB input by the Oligocene rather than Miocene provides stronger support for their hypothesis. The lack of unconformity in the forearc basin further south (Minbu Basin) may reflect the decreasing influence of collision in more southern distal settings.

The influence of the MMB then increased through time throughout the Oligo-Miocene, as evidenced by the increased proportion of metamorphic detritus, young zircons with negative εHf values and Cenozoic rutiles, and Sr-Nd signatures moving toward a higher proportion of old crustal material. This is consistent with the timing of exhumation of the MMB (Section 2.1). This gradual evolution of provenance with increase in the proportion of MMB through time since the Oligocene is at variance with the proposal of Westerweel et al. (2019). Those authors considered that MMB detritus first arrived on the WBT in the Miocene, above an unconformity between the Tonhe and Letkat formations, with both the unconformity and provenance change explained as due to indentation of the WBT into the eastern Himalayan syntaxis. With our alternative view, this then leaves a question over the cause of the unconformity in the CMB at the Oligo-Miocene boundary. We note that this time is coeval with a period of exhumation in the IBR (Najman et al., 2020, this paper Section 4.1.3) for which there may be a common cause.

5.2. Age Elevation Profiles

5.2.1. Tedim Age Elevation Transect

The time when the IBR core in the Tedim section (Zone T5) began to be exhumed is poorly constrained but appears to be older than the zones farther west. Zones T2, T3, and T4 were all heated beneath accumulating strata during the Eocene. Our thermal models do not have the resolution to detect small duration and short magnitude exhumation pulses during this time; however, all three zones were heated from deposition to over 170°C in this interval. The main phase of rapid exhumation occurred during the latest Oligocene—early Miocene. Rapid cooling starting in zone T3 around 25 Ma (∼26–20 Ma). Very rapid cooling started in zone T2 at ∼20 Ma and in zone T1 at ∼10 Ma. Therefore, deformation propagated generally westward from zone T4 to T1. The similar magnitude of exhumation in the first three of these four blocks suggests that the intervening Zunki and Thoubal

faults have limited vertical offsets. However, as zone T1 began to be exhumed more recently, we suggest that the Lemyo Fault must have been the most important structure controlling Oligo-Miocene shortening.

5.2.2. Refining the Mindat Age Elevation Transect of Najman et al. (2020)

We correlate Zone T5 of the Tedim profile with the Kanpetlet schist-bearing IBR core in the Mindat profile, where exhumation commenced at ~49 ± 3 Ma (Figures 2 and 4c). The onset of exhumation proposed in Najman et al. (2020) for the Mindat section, at or prior to 40 Ma, was estimated using age-elevation pseudo-vertical profiles. These profiles did not include ZFT data because it is hard to assign a precise closure temperature to ZFT data. In contrast, the QTQt models incorporate the ZFT data by limiting the temperature range that the model examines, and uses radiation damage-constrained ZHe models as well as the depositional ages of the samples. Therefore, they provide loose constraints on the heating paths and better define the inflection point delineating the transition from burial to exhumation. Our QTQt model of the Mindat IBR core (Figures 4c and 4d), now incorporating this additional information, confirms the Eocene pulse of cooling and refines the onset age to ~49 ± 3 Ma.

5.2.3. Discussion on Age Elevation Profile Data

In both our previously published and new age elevation profiles, a major period of exhumation occurs at the time of the Oligo-Miocene boundary. Previously we suggested that the cause of this exhumation episode may have been a change in wedge dynamics associated with increased sedimentation to the system from the Bengal Fan (Najman et al., 2020; Luan et al., 2021). Additionally, our new data from the Mindat profile strengthen our Tedim data set, indicating another period of exhumation of the IBR in the early-middle Eocene, now dated around ~49 ± 3 Ma. Exhumation at both sections was likely controlled by the west-vergent Kheng fault, west of the IBR core. This exhumation event may be related to the timing of collision between the WBT and India, as constrained by paleomagnetic data, considered by Westerweel et al. (2019) to show collision around 40 Ma, with later refinement (Westerweel, 2020 quoted in Morley et al., 2021, their Figure 3d) indicating collision may be as old as 50 Ma. However, for both Oligo-Miocene and Eocene events, other previously proposed mechanisms remain equally valid, for example, a change in angle of the subducting slab, the influence of the prism's location in a hyper-oblique setting with localized strain partitioning, changes in plate kinematics, impact of the 90E Ridge, or collision of the WBT with a small allochthonous terrane or island arc (see reviews in Licht et al., 2018 and in Morley and Arboit, 2019, and papers by Acharyya, 2015; Maurin and Rangin, 2009; Li et al., 2018).

6. Conclusions

Our provenance data from the CMB indicate that detritus from the MMB and spatially associated granites was first deposited in the CMB of the WBT after the early part of the late Eocene and by the early Oligocene, based on a lack of such material in the earliest upper Eocene rocks and its presence in lower Oligocene strata. These results provide a minimum age constraint to the timing of WBT-Asia collision, which may also be responsible for the unconformity observed in the CMB at this time. We interpret that any potential earlier provenance change was related to influx from basement material within the WBT rather than influx from the MMB.

Our low temperature thermochronology data from the IBR record periods of exhumation in the early-middle Eocene and around the Oligo-Miocene boundary. The early-middle Eocene period of exhumation may be associated with the collision of WBT with India. In Najman et al. (2020), we proposed that the major period of exhumation at the Oligo-Miocene boundary may be related to a change in wedge dynamics associated with increased sedimentation to the system from the Bengal Fan. However, we note that for both the Eocene and Oligo-Miocene events, a number of other viable proposed mechanisms remain.

Data Availability Statement

Data is accessible in supporting information for review purposes and will be made available on figshare at https://doi.org/10.6084/m9.figshare.17283962 upon acceptance.

Acknowledgments
We thank the guides and drivers in Myanmar for enabling the field work and technical staff at NIGL for analytical support. Discussions with Alexis Licht (CNRS, Aix-en-Provence, France), Chris Morley (Chiang Mai University, Thailand), Shihu Li (Chinese Academy of Sciences, Beijing), Pierrick Roperch and Jan Westerweel (University of Rennes) helped clarify our ideas. Constructive reviews from Alexis Licht, Pierrick Roperch and an anonymous reviewer improved the quality of this submission. This work is supported by National Natural Science Foundation of China (No. 92055211), China-ASEAN Maritime Cooperation Fund Project (No. 12120100500017001).

References

Acharyya, S. K. (2015). Indo-Burma Range: A belt of accreted microcontinents, ophiolites and mesozoic-paleogene flyschoid sediments. *International Journal of Earth Sciences*, *104*(5), 1235–1251. https://doi.org/10.1007/s00531-015-1154-6

Aitchison, J. C., Ali, J. R., & Davis, A. M. (2007). When and where did India and Asia collide? *Journal of Geophysical Research*, *112*, B05423. https://doi.org/10.1029/02006JB004706

Aitchison, J. C., Ao, A., Bhowmik, S., Clarke, G. L., Ireland, T. R., Kachovich, S., et al. (2019). Tectonic evolution of the western margin of the Burma microplate based on new fossil and radiometric age constraints. *Tectonics*, *38*(5), 1718–1741. https://doi.org/10.1029/2018TC005049

Andò, S., Morton, A., & Garzanti, E. (2014). Metamorphic grade of source rocks revealed by chemical fingerprints of detrital amphibole and garnet. In R. A. Scott, H. R. Smyth, A. C. Morton, & N. Richardson (Eds.), *Sediment provenance studies in hydrocarbon exploration and production* (pp. 351–371). Geological Society London, Special Publication.

Arboit, F., Min, M., Chew, D., Mitchell, A., Drost, K., Badenszki, E., & Daly, J. S. (2021). Constraining the links between the Himalayan belt and the Central Myanmar Basins during the Cenozoic: An integrated multi-proxy detrital geochronology and trace-element geochemistry study. *Geoscience Frontiers*, *12*(2), 657–676. https://doi.org/10.1016/j.gsf.2020.05.024

Bannert, D., Sang Lyen, A., & Htay, T. (2012). *The geology of the Indoburman Ranges in Myanmar*. Geologisches Jahrbuch.

Barber, A. J., Zaw, K., & Crow, M. J. (2017). The pre-Cenozoic tectonic evolution of Myanmar. In A. J. Barber, K. Zaw, & M. J. Crow (Eds.), *Myanmar; geology, resources and tectonics* (pp. 687–712). Geological Society of London, Memoirs.

Barley, M. E., Pickard, A. L., Zaw, K., Rak, P., & Doyle, M. G. (2003). Jurassic to Miocene magmatism and metamorphism in the Mogok metamorphic belt and the India-Eurasia collision in Myanmar. *Tectonics*, *22*(3). https://doi.org/10.1029/2002tc001398

Bender, F. (1983). *Geology of Burma*. Borntraeger.

Bertrand, G., Rangin, C., Maluski, H., & Bellon, H. (2001). Diachronous cooling along the Mogok Metamorphic Belt (Shan Scarp, Myanmar): The trace of the northward migration of the Indian syntaxis. *Journal of Asian Earth Sciences*, *19*(5), 649–659. https://doi.org/10.1016/S1367-9120(00)00061-4

Betka, P. M., Seeber, L., Thomson, S. N., Steckler, M. S., Sincavage, R., & Zoramthara, C. (2018). Slip-partitioning above a shallow, weak decollement beneath the Indo-Burman accretionary prism. *Earth and Planetary Science Letters*, *503*, 17–28. https://doi.org/10.1016/j.epsl.2018.09.003

Betka, P. M., Thomson, S. N., Sincavage, R., Zoramthara, C., Lalremruatfela, C., Lang, K. A., et al. (2021). Provenance shifts during Neogene Brahmaputra delta progradation tied to coupled climate and tectonic change in the Eastern Himalaya. *Geochemistry, Geophysics, Geosystems*, *22*, e2021GC010026. https://doi.org/10.1029/2021gc010026

Bracciali, L., Najman, Y., Parrish, R. R., Akhter, S. H., & Millar, I. (2015). The Brahmaputra tale of tectonics and erosion: Early Miocene river capture in the Eastern Himalaya. *Earth and Planetary Science Letters*, *415*, 25–37. https://doi.org/10.1016/j.epsl.2015.01.022

Bracciali, L., Parrish, R., Horstwood, M., Condon, D., & Najman, Y. (2013). U-Pb LA-(MC)-ICP-MS dating of rutile: New reference materials and applications to sedimentary provenance. *Chemical Geology*, *347*, 82–101. https://doi.org/10.1016/j.chemgeo.2013.03.013

Brunnschweiler, R. O. (1966). On the geology of the Indoburman ranges. *Journal of the Geological Society of Australia*, *13*, 137–194. https://doi.org/10.1080/00167616608728608

Burma Earth Sciences Research Division, B. (1977). *Geological map of the Socialist Republic of the Union of Burma, 1:1000000*. Security Printing Works, Burma.

Cai, F. L., Ding, L., Zhang, Q. H., Orme, D. A., Wei, H. H., Li, J. X., et al. (2020). Initiation and evolution of forearc basins in the Central Myanmar Depression. *The Geological Society of America Bulletin*, *132*(5–6), 1066–1082. https://doi.org/10.1130/B35301.1

Galetto, A. V., Georgieva, V., Garcia, V. H., Zattin, M., Sobel, E. R., Glodny, J., et al. (2021). Cretaceous and Eocene rapid cooling phases in the Southern Andes (36°–37°S): Insights from low-temperature thermochronology, U-Pb geochronology, and inverse thermal modeling from Domuyo area, Argentina. *Tectonics*, *40*. https://doi.org/10.1029/2020TC006415

Gallagher, K. (2012). Transdimensional inverse thermal history modeling for quantitative thermochronology. *Journal of Geophysical Research*, *117*, B02408. https://doi.org/10.01029/02011JB008825

Gardiner, N. J., Searle, M. P., Morley, C. K., Robb, L. J., Whitehouse, M. J., Roberts, N. M. W., et al. (2018). The crustal architecture of Myanmar imaged through zircon U-Pb, Lu-Hf and O isotopes: Tectonic and metallogenic implications. *Gondwana Research*, *62*, 27–60. https://doi.org/10.1016/j.gr.2018.02.008

Garzanti, E. (2019). Petrographic classification of sand and sandstone. *Earth-Science Reviews*, *190*, 545–563. https://doi.org/10.1016/j.earscirev.2018.1012.1014

Garzanti, E., & Vezzoli, G. (2003). A classification of metamorphic grade in sands based on their composition and grade. *Journal of Sedimentary Research*, *73*, 830–837. https://doi.org/10.1306/012203730830

Ghose, N., Chatterjee, N., & Fareeduddin. (2014). *A petrographic atlas of ophiolite: An example from the eastern India-Asia collision zone*. Springer.

Guenthner, W. R., Reiners, P. W., Ketcham, R. A., Nasdala, L., & Giester, G. (2013). Helium diffusion in natural zircon: Radiation damage, anisotropy, and the interpretation of zircon (U-Th)/He thermochronology. *American Journal of Science*, *313*, 145–198. https://doi.org/10.2475/03.2013.01

Guo, R., Hu, X., Garzanti, E., Lai, W., Yan, B., & Mark, C. (2020). How faithfully do the geochronological and geochemical signatures of detrital zircon, titanite, rutile and monazite record magmatic and metamorphic events? A case study from the Himalaya and Tibet. *Earth-Science Reviews*, *201*, 103082. https://doi.org/10.1016/j.earscirev.2020.103082

Hall, R. (2012). Late Jurassic-Cenozoic reconstructions of the Indonesian region and the Indian ocean. *Tectonophysics*, *570*, 1–41. https://doi.org/10.1016/j.tecto.2012.04.021

Handique, G. K., Sethi, A. K., & Sarma, S. C. (1989). *Review of tertiary stratigraphy of parts of upper Assam valley* (Vol. 23, pp. 23–36). Geological Survey of India Publication.

Horstwood, M. S. A., Kosler, J., Gehrels, G., Jackson, S. E., McLean, N. M., Paton, C., et al. (2016). Community-derived standards for LA-ICP-MS U-(Th-)Pb geochronology—Uncertainty propagation, age interpretation and data reporting. *Geostandards and Geoanalytical Research*, *40*(3), 311–332. https://doi.org/10.1111/j.1751-908X.2016.00379.x

Htut, T. (2017). Myanmar Petroleum Systems, including the offshore area. In A. J. Barber, K. Zaw, & M. J. Crow (Eds.), *Myanmar: Geology, resources and tectonics* (pp. 219–260). Geological Society of London Memors.

Ingersoll, R. V., Bullard, T. F., Ford, R. L., Grimm, J. P., Pickle, J. D., & Sares, S. W. (1984). The effect of grain-size on detrital modes: A test of the Gazzi-Dickinson point-counting method. *Journal of Sedimentary Petrology*, *54*, 103–116. https://doi.org/10.1306/212F83B9-2B24-11D7-8648000102C1865D

Lamont, T. N., Searle, M. P., Hacker, B. R., Htun, K., Htun, K. M., Morley, C. K., et al. (2021). Late Eocene-Oligocene granulite facies garnet-sillimanite migmatites from the Mogok Metamorphic belt, Myanmar, and implications for timing of slip along the Sagaing Fault. *Lithos*, *386–387*, 386. https://doi.org/10.1016/j.lithos.2021.106027

Li, J.-X., Fan, W.-M., Zhang, L.-Y., Evans, N. J., Sun, Y.-L., Guan, Q.-Y., et al. (2019). Geochronology, geochemistry and Sr-Nd-Hf isotopic compositions of Late Cretaceous-Eocene granites in southern Myanmar: Petrogenetic, tectonic and metallogenic implications. *Ore Geology Reviews*, *112*, 103031. https://doi.org/10.1016/j.oregeorev.2019.103031

Li, J.-X., Fan, W.-M., Zhang, L.-Y., Peng, T.-P., Sun, Y.-L., Ding, L., et al. (2020). Prolonged Neo-Tethyan magmatic arc in Myanmar: Evidence from geochemistry and Sr-Nd-Hf isotopes of Cretaceous mafic-felsic intrusions in the Banmauk-Kawlin area. *International Journal of Earth Sciences*, *109*, 649–668. https://doi.org/10.1007/s00531-020-01824-w

Li, S. H., van Hinsbergen, D. J. J., Deng, C. L., Advokaat, E. L., & Zhu, R. X. (2018). Paleomagnetic constraints from the Baoshan area on the deformation of the Qiangtang-Sibumasu terrane around the eastern Himalayan syntaxis. *Journal of Geophysical Research: Solid Earth*, *123*(2), 977–997.

Liang, Y.-H., Chung, S. L., Liu, D., Xu, Y., Wu, F. Y., Yang, J. H., et al. (2008). Detrital zircon evidence from Burma for reorganisation of the eastern Himalayan drainage system. *American Journal of Science*, *308*, 618–638. https://doi.org/10.2475/04.2008.08

Licht, A., Dupont-Nivet, G., Win, Z., Swe, H. H., Kaythi, M., Roperch, P., et al. (2018). Paleogene evolution of the Burmese forearc basin and implications for the history of India-Asia convergence. *The Geological Society of America Bulletin*, *131*, 730–748. https://doi.org/10.1130/B35002.1

Licht, A., France-Lanord, C., Reisberg, L., Fontaine, C., Soe, A. N., & Jaeger, J. J. (2013). A palaeo Tibet-Myanmar connection? Reconstructing the late Eocene drainage system of central Myanmar using a multi-proxy approach. *Journal of the Geological Society*, *170*(6), 929–939. https://doi.org/10.1144/jgs2012-126

Licht, A., Reisberg, L., France-Lanord, C., Naing Soe, A., & Jaeger, J. J. (2014). Cenozoic evolution of the central Myanmar drainage system: Insights from sediment provenance in the Minbu Sub-Basin. *Basin Research*, *28*, 237–251. https://doi.org/10.1111/bre.12108

Licht, A., Win, Z., Westerweel, J., Cogne, N., Morley, C. K., Chantraprasert, S., et al. (2020). Magmatic history of central Myanmar and implications for the evolution of the Burma Terrane. *Gondwana Research*, *87*, 303–319. https://doi.org/10.1016/j.gr.2020.06.016

Lin, T.-H., Mitchell, A. H. G., Chung, S.-L., Tan, X.-B., Tang, J.-T., Oo, T., & Wu, F.-Y. (2019). Two parallel magmatic belts with contrasting isotopic characteristics from southern tibet to Myanmar: Zircon U–Pb and Hf isotopic constraints. *Journal of the Geological Society*, *176*, 574–587. https://doi.org/10.1144/jgs2018-072

Liu, C.-Z., Chung, S.-L., Wu, F.-Y., Zhang, C., Xu, Y., Wang, J.-G., et al. (2016). Tethyan suturing in Southeast Asia: Zircon U-Pb and Hf-O isotopic constraints from Myanmar ophiolites. *Geology*, *44*(4), 311–314. https://doi.org/10.1130/g37342.1

Luan, X., Islam, M. S., Wei, X., Lu, Y., Fan, G., Pau, S. K., & Lwin, S. M. (2021). Hydrocarbon accumulation in and active accretionary prism, a case study in the deepwater Rakhine Basin, Myanmar offshore. *Journal of Asian Earth Sciences*, *221*, 104941. https://doi.org/10.1016/j.jseaes.2021.104941

Luvizotto, G., Zack, T., Meyer, H., Ludwig, T., Triebold, S., Kronz, A., et al. (2009). Rutile crystals as potential trace element and isotope mineral standards for microanalysis. *Chemical Geology*, *261*(3), 346–369.

Maurin, T., & Rangin, C. (2009). Impact of the 90°E ridge at the Indo-Burmese subduction zone imaged from deep seismic reflection data. *Marine Geology*, *266*(1–4), 143–155. https://doi.org/10.1016/j.margeo.2009.07.015

Mitchell, A. (2018). *Geological belts, plate boundaries, and mineral deposits in Myanmar*. Elsevier.

Mitchell, A. H. G., Chung, S.-L., Thura, O., Lin, T.-S., & Hung, C.-H. (2012). Zircon U-Pb ages in Myanmar: Magmatic-metamorphic events and the closure of a Neotethys ocean? *Journal of Asian Earth Sciences*, *56*, 1–23. https://doi.org/10.1016/j.jseaes.2012.04.019

Mitchell, A. H. G., Hlaing, T., & Htay, N. (2010). The Chin Hills segment of the Indo-Burman Ranges: Not a simple accretionary wedge. *Memoir, Geological Society of India*, *75*, 3–24.

Morley, C. K. (2009). Evolution from an oblique subduction back-arc mobile belt to a highly oblique collisional margin: The Cenozoic tectonic development of Thailand and eastern Myanmar. *Geological Society London Special Publication*, *318*, 373–403. https://doi.org/10.1144/sp318.14

Morley, C. K., & Arboit, F. (2019). Dating the onset of motion on the Sagaing fault: Evidence from detrital zircon and titanite U-Pb geochronology from the North Minwun Basin, Myanmar. *Geology*, *47*(6), 581–585. https://doi.org/10.1130/G46321.1

Morley, C. K., Chantraprasert, S., Kongchum, J., & Chenoll, K. (2021). The West Burma Terrane, a review of recent paleo-latitude data, its geological implications and constraints. *Earth-Science Reviews*, *220*, 103722. https://doi.org/10.1016/j.earscirev.2021.103722

Morley, C. K., Naing, T. T., Searle, M., & Robinson, S. A. (2020). Structural and tectonic development of the Indo-Burma Ranges. *Earth-Science Reviews*, *200*, 102992. https://doi.org/10.1016/j.earscirev.2019.102992

Naing, T. T., Bussien, D. A., Winkler, W. H., Nold, M., & Von Quadt, A. (2014). Provenance study on Eocene-Miocene sandstones of the Rakhine coastal belt, Indo-Burman Ranges of Myanmar: Geodynamic implications. In R. A. Scott, H. R. Smyth, A. C. Morton, & N. Richardson (Eds.), *Sediment provenance studies in hydrocarbon exploration and production* (pp. 195–216). Geological Society, London, Special Publications.

Najman, Y., Bickle, M., BouDagher-Fadel, M., Carter, A., Garzanti, E., Paul, M., et al. (2008). The Paleogene record of Himalayan erosion: Bengal Basin, Bangladesh. *Earth and Planetary Science Letters*, *273*(1–2), 1–14. https://doi.org/10.1016/j.epsl.2008.04.028

Najman, Y., Sobel, E. R., Millar, I., Stockli, D. F., Govin, G., Lisker, F., et al. (2020). The exhumation of the Indo-Burman Ranges, Myanmar. *Earth and Planetary Science Letters*, *530*, 115948. https://doi.org/10.1016/j.epsl.2019.115948

Parra, M., Mora, A., Sobel, E. R., Strecker, M. R., & González, R. (2009). Episodic orogenic front migration in the northern Andes: Constraints from low-temperature thermochronology in the Eastern Cordillera, Colombia. *Tectonics*, *28*, TC4004. https://doi.org/10.1029/2008TC002423

Paton, C., Hellstrom, J., Paul, B., Woodhead, J., & Hergt, J. (2011). Iolite: Freeware for the visualisation and processing of mass spectrometric data. *Journal of Analytical Atomic Spectrometry*, *26*(12), 2508–2518.

Rangin, C., Maurin, T., & Masson, F. (2013). Combined effects of Eurasia/Sunda oblique convergence and East-Tibetan crustal flow on the active tectonics of Burma. *Journal of Asian Earth Sciences*, *76*, 185–194. https://doi.org/10.1016/j.jseaes.2013.05.018

Reiners, P. W., & Brandon, M. T. (2006). Using thermochronology to understand orogenic erosion. *Annual Review of Earth and Planetary Sciences*, *34*, 419–466. https://doi.org/10.1146/annurev.earth.34.031405.125202

Robinson, R. A. J., Brezina, C. A., Parrish, R. R., Horstwood, M. S. A., Oo, N. W., Bird, M. I., et al. (2014). Large rivers and orogens: The evolution of the Yarlung Tsangpo-Irrawaddy system and the eastern Himalayan syntaxis. *Gondwana Research*, *26*(1), 112–121. https://doi.org/10.1016/j.gr.2013.07.002

Searle, M. P., Garber, J. M., Hacker, B. R., Htun, K., Gardiner, N. J., Waters, D. J., & Robb, L. J. (2020). Timing of Syenite-charnockite magmatism and ruby and Sapphire metamorphism in the Mogok Valley Region, Myanmar. *Tectonics*, *39*(3). https://doi.org/10.1029/2019tc005998

Singh, A. K., Chung, S.-L., Bikramaditya, R. K., & Lee, H. Y. (2016). New U–Pb zircon ages of plagiogranites from the Nagaland–Manipur Ophiolites, Indo-Myanmar Orogenic Belt, NE India. *Journal of the Geological Society*, *174*(1), 170–179. https://doi.org/10.1144/jgs2016-048

Sláma, J., Košler, J., Condon, D. J., Crowley, J. L., Gerdes, A., Hanchar, J. M., et al. (2008). Plešovice zircon—A new natural reference material for U–Pb and Hf isotopic microanalysis. *Chemical Geology*, *249*(1), 1–35. https://doi.org/10.1016/j.chemgeo.2007.11.005

Sobel, E. R., & Strecker, M. R. (2003). Uplift, exhumation and precipitation: Tectonic and climatic control of Late Cenozoic landscape evolution in the northern Sierras Pampeanas, Argentina. *Basin Research*, *15*(4), 431–451. https://doi.org/10.1046/j.1365-2117.2003.00214.x

Socquet, A., Goffe, B., Pubellier, M., & Ragin, C. (2002). Le metamorphism Tardi-Cretace a Eocene des zones internes de la chaine Indo-Birmane (Myanmar Occidental): Implications Geodynamiques. *Comptes Rendus Geoscience*, *334*, 573–580. https://doi.org/10.1016/s1631-0713(02)01796-0

Verard, C., Stampfli, G., Borel, G., & Hochard, C. (2017). The Indian promontory: A bridge between plate tectonics and life evolution models. *Universal Journal of Geoscience*, *5*, 25–32. https://doi.org/10.13189/ujg.2017.050202

Vermeesch, P. (2018). IsoplotR: A free and open toolbox for geochronology. *Geoscience Frontiers*, *9*, 1479–1493. https://doi.org/10.1016/j.gsf.2018.04.001

Wang, J. G., Wu, F. Y., Tan, X. C., & Liu, C. Z. (2014). Magmatic evolution of the Western Myanmar Arc documented by U-Pb and Hf isotopes in detrital zircon. *Tectonophysics*, *612*, 97–105. https://doi.org/10.1016/j.tecto.2013.11.039

Westerweel, J. (2020). *The India-Asia collision from the perspective of Myanmar: Insights from paleomagnetism and paleogeographic reconstructions*. University of Rennes.

Westerweel, J., Licht, A., Cogne, N., Roperch, P., Dupont-Nivet, G., Thi, M. K., et al. (2020). Burma terrane collision and northward indentation in the Eastern Himalayas recorded in the Eocene-Miocene Chindwin Basin (Myanmar). *Tectonics*, *39*(10), e2020TC006413. https://doi.org/10.1029/2020tc006413

Westerweel, J., Roperch, P., Licht, A., Dupont-Nivet, G., Win, Z., Poblete, F., et al. (2019). Burma Terrane part of the Trans-Tethyan arc during collision with India according to palaeomagnetic data. *Nature Geoscience*, *12*(10), 863–868. https://doi.org/10.1038/s41561-019-0443-2

Wiedenbeck, M., Alle, P., Corfu, F., Griffin, W., Meier, M., Oberli, F., et al. (1995). Three natural zircon standards for U-Th-Pb, Lu-Hf, trace element and REE analyses. *Geostandards Newsletter*, *19*(1), 1–23. https://doi.org/10.1111/j.1751-908X.1995.tb00147.x

Yao, W., Ding, L., Cai, F., Wang, H., Xu, Q., & Zaw, T. (2017). Origin and tectonic evolution of upper Triassic Turbidites in the Indo-Burman Ranges, West Myanmar. *Tectonophysics*, *721*, 90–105. https://doi.org/10.1016/j.tecto.2017.09.016

Zack, T., Stockli, D. F., Luvizotto, G. L., Barth, M. G., Belousova, E., Wolfe, M. R., & Hinton, R. W. (2011). In situ U-Pb rutile dating by LA-ICP-MS: ^{208}Pb correction and prospects for geological applications. *Contributions to Mineralogy and Petrology*, *162*, 515–530. https://doi.org/10.1007/s00410-011-0609-4

Zhang, J., Xiao, W., Windley, B. F., Cai, F., Sein, K., & Naing, S. (2017). Early cretaceous wedge extrusion in the Indo-Burma Range accretionary complex: Implications for the Mesozoic subduction of Neothethys in SE Asia. *International Journal of Earth Sciences*, *106*, 1391–1408. https://doi.org/10.1007/s00531-017-1468-7

Zhang, P., Mei, L. F., Hu, X. L., Li, R. Y., Wu, L. L., Zhou, Z. C., & Qiu, H. N. (2017). Structures, uplift, and magmatism of the Western Myanmar Arc: Constraints to mid-Cretaceous-Paleogene tectonic evolution of the Western Myanmar continental margin. *Gondwana Research*, *52*, 18–38. https://doi.org/10.1016/j.gr.2017.09.002

Zhang, P., Mei, L. F., Jiang, S. Y., Xu, S. H., Donelick, R. A., Li, R. Y., & Zhang, H. (2021). Erosion and sedimentation in SE Tibet and Myanmar during the evolution of the Burmese continental margin from the Late Cretaceous to Early Neogene. *Gondwana Research*, *95*, 149–175. https://doi.org/10.1016/j.gr.2021.04.005

Zhao, S.-W., Lai, S.-C., Qin, J.-F., Zhu, R.-Z., & Wang, J.-B. (2017). Geochemical and geochronological characteristics of Late Cretaceous to Early Paleocene granitoids in the Tengchong Block, Southwestern China: Implications for crustal anatexis and thickness variations along the eastern Neo-Tethys subduction zone. *Tectonophysics*, *694*, 87–100. https://doi.org/10.1016/j.tecto.2016.11.038

Zhou, R., Schoenbohm, L. M., Sobel, E., Davis, D. W., & Glodny, J. (2017). New constraints on orogenic models of the southern Central Andean Plateau: Cenozoic basin evolution and bedrock exhumation. *The Geological Society of America Bulletin*, *129*, 152–170. https://doi.org/10.1130/b31384.1